MeMoVolc consensual document: a review of cross-disciplinary approaches to characterizing small explosive magmatic eruptions

L. Gurioli[1], D. Andronico[2], P. Bachelery[1], H. Balcone-Boissard[3], J. Battaglia[1], G. Boudon[4], A. Burgisser[5], S.B. M.R. Burton[6], K. Cashman[7], S. Cichy[1], R. Cioni[8], A. Di Muro[9], L. Dominguez[10], C. D'Oriano[6], T. Druitt[1], A.J.L Harris[1], M. Hort[11], K. Kelfoun[1], J.C. Komorowski[4], U. Kueppers[12], J.L. Le Pennec[1], T. Menand[1], R. Paris[1], L. Pioli[10], M. Pistolesi[13], M. Polacci[6], M. Pompilio[6], M. Ripepe[8], O. Roche[1], E. Rose-Koga[1], A. Rust[7], F. Schiavi[1], L. Sharff[11], R. Sulpizio[14], J. Taddeucci[15], T. Thordarson[16]

1 Laboratoire Magmas et Volcans, Université Blaise Pascal - CNRS - IRD, OPGC, 5 rue Kessler, 63038 Clermont Ferrand, France
2 INGV, Osservatorio Etneo, Sezione di Catania, 95125 Catania, Italy
3 Sorbonne Universités, UPMC Univ Paris 06, UMR 7193, Institut des Sciences de la Terre Paris (iSTeP) and CNRS, F-75005 Paris, France
4 Institut de Physique du Globe (IPGP), Sorbonne Paris-Cité, Université Paris Diderot, CNRS UMR-7154, 1 rue Jussieu, 75238 Paris Cedex 05, France
5 ISTerre Université de Savoie CNRS, 73376 Le Bourget du lac, France
6 INGV, Sezione di Pisa, 56126 Pisa, Italy
7 School of Earth Sciences, University of Bristol, United Kingdom
8 Dipartimento di Scienze della Terra, Università degli Studi di Firenze, 50121 Florence, Italy
9 Institut de Physique du Globe (IPGP), Sorbonne Paris-Cité, CNRS UMR-7154, Université Paris Diderot, Observatoire Volcanologique du Piton de la Fournaise (OVPF), Bourg Murat, France
10 Département de Minéralogie, Université de Genève, Switzerland
11 Klimacampus, CEN, University of Hamburg, Germany
12 Ludwig-Maximilians-Universitaet (LMU), Munich, Germany
13 Dipartimento Scienze della Terra, Università degli Studi di Pisa, Italy
14 Dipartimento di Scienze della Terra e Geo-Ambientali, Università degli Studi di Bari, Italy
15 INGV, Sezione di Roma, 00143 Roma, Italy
16 Institute of Earth Sciences (IES), University of Iceland, Reykjavík, Iceland

Abstract A workshop entitled "*Tracking and understanding volcanic emissions through cross-disciplinary integration: A textural working group*." was held at the Université Blaise Pascal (Clermont-Ferrand, France) on the 6-7 November 2012. This workshop was supported by the European Science Foundation (ESF). The main objective of the workshop was to

establish an initial advisory group to begin to define measurements, methods, formats and standards to be applied in the integration of geophysical, physical and textural data collected during volcanic eruptions. This would homogenize procedures to be applied and integrated during both past and ongoing events. The workshop comprised a total of 35 scientists from six countries (France, Italy, Great Britain, Germany, Switzerland and Iceland). The four main aims were to discuss and define:

- Standards, precision and measurement protocols for textural analysis
- Identification of textural, field deposit, chemistry and geophysical parameters that can best be measured and combined
- The best delivery formats so that data can be shared between, and easily used by different groups;
- Multi-disciplinary sampling and measurement routines currently used, and measurement standards applied, by each community

The group agreed that community-wide, cross-disciplinary integration, centered on defining those measurements and formats that can be best combined, is an attainable and key global focus. Consequently, we prepared this paper to present our initial conclusions and recommendations, along with a review of the current state of the art in this field that supported our discussions.

Introduction

A major goal of modern volcanology is to relate conditions of magma ascent to the resulting eruption style using information preserved in volcanic deposits. Because it is impossible to directly observe magma ascent, vesiculation and fragmentation, one way to obtain quantitative information on magma-ascent dynamics is through textural quantification of the sampled particles. Textural quantification involves full description of the vesicle and crystal properties of erupted products (e.g., Sparks 1978; Sparks and Brazier 1982; Whitham and Sparks 1986; Houghton and Wilson 1989; Marsh 1988, 1998; Cashman and Marsh 1988, Toramaru 1989, 1990; Cashman and Mangan 1994; Higgins 2000; 2006; Blower et al. 2002; Burgisser and Gardner 2005; Shea et al. 2010a; Rust and Cashman 2011; Baker et al. 2012 and references therein). Magma viscosity, ascent rate, vesiculation processes, fragmentation style and explosion dynamics all imprint characteristic and measurable properties on the textures of volcanic particles, as shown by theoretical and experimental studies (e.g., Rust and

Cashman 2011; Gonnerman and Houghton 2012; Degruyter et al. 2012; Nguyen et al. 2013 and references therein). The main assumption is that most of the pyroclast properties are acquired during ascent in the conduit, with few changes occurring after fragmentation or in the atmosphere, if the pyroclasts are lapilli size or smaller (e.g., Houghton and Wilson 1989; Nguyen et al. 2013). Specifically, the textural parameters of the pyroclastic components can yield insights into the dynamics of explosive eruptions, as reviewed in Table 1.

However, the physical characteristics of individual pyroclasts must not be considered in isolation from detailed studies of (i) the deposits from which they were collected, (ii) their chemical properties, (iii) geophysical signatures of the related explosive event, or (iv) petrological and/or analogue experiments. Indeed, attempts to understand eruption dynamics have been increasingly coupled to traditional fieldwork and geophysical measurements made synchronously with sample collection. In 2004, a special issue of the *Journal of Volcanology and Geothermal Research* (Volume 137) focused on multidisciplinary approaches, proposing "*simultaneous collection of multiple geophysical data sets, such as seismic, infrasonic, thermal and deformation data, as well as sampling of ejecta and detailed mapping*". The argument was that "*complete constraint of a volcanic system is not possible using one data set, so that an integrated multiparametric approach involving simultaneous collection of multiple geophysical and petrological data sets will increase our ability to reach tightly constrained and confident conclusions regarding the mechanics and dynamics of volcanic systems and eruptions*" (Harris et al. 2004). Since 2004, numerous studies have borne these predictions out, combining textural data with:

i. Field deposits (e.g., Polacci et al. 2006a; Rust and Cashman 2007; 2011; Mattsson 2010);
ii. Petrological data (e.g., Larsen 2008; Shea et al. 2009; 2010b; Burgisser et al. 2010; Bai et al. 2011);
iii. Chemical analyses (e.g., Piochi et al. 2005, 2008; Shimano and Nakada 2006; Noguchi et al. 2006; Costantini et al. 2010; Schipper et al. 2010a; b; c; 2011; 2012; 2013; Balcone-Boissard et al. 2010, 2011, 2012; Shea et al. 2012; 2014)
iv. Geophysical measurements (e.g., Burton et al. 2007; Gurioli et al. 2008, 2013; 2014; Polacci et al. 2009b; Andronico et al. 2008; 2009a; 2009b; 2013a, 2013b; Miwa et al. 2009; Miwa and Toramaru 2013; Colò et al. 2010; Landi et al. 2011; Pistolesi et al. 2011; Leduc et al. 2015)

Together, these studies have delivered complete pictures of explosive eruptions and their dynamics (Fig. 1).

Despite this progress, we remain far from establishing the best protocols for sampling pyroclasts and for correlating and comparing the many parameters that can be measured using individual clasts and field deposits. Only a few papers address some of these issues (e.g., Bonadonna et al 2013; Engwell et al. 2013; Klawon et al. 2014). In addition, no study has yet attempted to correlate all derivable textural parameters with the full range of multidisciplinary data available. To partially resolve these issues, a working group funded by the European Science Foundation, through the MeMoVolc program (http://www.memovolc.fr/), was set up. The group was composed of experts actively working on integration of textural, deposit and geophysical data, equally balanced between four theme areas: (i) particle-texture studies, (ii) deposit analysis, (iii) chemistry and (iv) geophysics. The priorities of the meeting were discussion and definition of:

- Improved standards, precision and measurement protocols needed by the particle-texture studies.
- Best practices for particle-texture studies in order to have comparable datasets from different types of eruptions.
- Parameters obtained from particle-texture, deposit, geochemical and geophysical data that need to be measured, and the best delivery format if each discipline's output is to be of use to all workers.
- Multi-disciplinary sampling and measurement routines, as well as measurement standards.

The core communal issues to be explored were agreed on:

1. What are the best sampling and measurement strategies for the quantification of pyroclast textural features, and what are their precision and uncertainty?
2. What are the best sampling and measurement strategies for pyroclastic deposits to allow textural characterization of their particles?
3. How can we link chemistry and particle-texture properties?
4. How can we link geophysical data and the particle-texture quantification?
5. What is the best multi-disciplinary strategy for combining output from each field in a meaningful way?

The paper reviews these topics in the light of a workshop consensus. Because of the time constraints and the complexity of the arguments, the paper focuses only on the study of explosive subaerial magmatic eruptions that generate sustained columns or fountains, and the associated fallout deposits (Fig. 1). Further workshop or working groups should be organized

to synthesise and integrate all work in progress, and already completed, in the areas of phreatic, phreatomagmatic and submarine explosions, as well as pyroclastic density current and lava flow deposits (Table 1). .

The final objective of this paper is to ensure that data collected in the field and laboratory can be shared effectively and ingested in a multi-disciplinary sense into experiments, modeling and monitoring. In the longer term, the objective is to publish and update standards, as well as to propose, support and organize field meetings to test integrated collection methodologies. The ultimate aim is to increase the number of open-access data-bases of standard and community-accepted quality, thereby increasing resources available for cross-disciplinary correlations.

Sampling of pyroclasts and quantification of their textural features

(i) Representative samples

Pyroclasts reflect degassing of the parent magma, from the conduit to the plume. Part of the textural signature is assumed to reflect the fragmentation (or explosion) zone. Consequently, texture can be used as an indicator of magma properties (composition, porosity, connectivity, permeability, vesicle and crystal content, size, shape and distribution) at that time (Table 1). This assumption has two requirements:

i. The textural signature that was quenched immediately at the fragmentation level can be distinguished from the textural effects of post-fragmentation processes, including microlite formation and bubble nucleation, expansion, collapse, coalescence and Ostwald ripening that will change clast vesicularity or vesicle size and shapes once the pyroclast has been formed (e.g., Thomas et al. 1994; Cashman et al. 1994; Herd and Pinkerton 1997; Larsen and Gardner 2000; Gurioli et al. 2008; Costantini et al. 2010; Stovall et al. 2011, 2012). The time window for post-fragmentation changes depends on magma composition, viscosity and fragmentation depth.
ii. Because clast density is also a function of clast size (Houghton and Wilson 1989), only clasts of similar sizes must be used in order to avoid non-uniform grain-size effects on textural parameters.

We thus recommend choosing samples that are representative of the studied explosion, or unit, in terms of:

i. Timing: This requires sampling of narrow stratigraphic intervals (Houghton and Wilson 1989) in which juvenile clasts of similar dimensions can be assumed to represent those parts of the magma fragmented at a particular time (n.b. conduit processes can change over short timescales);
ii. Distribution: This requires selection of more than one outcrop for each event;
iii. Degree of fragmentation: This requires selection of a sampling methods that is appropriate for the the full range of grain sizes in the deposit;
iv. Componentry: If the juvenile fraction is heterogeneous, then sampling should be done based on preliminary componentry analysis of the clasts analyzed (e.g., Wright et al. 2011, Eychenne et al 2015)

In previous studies, only clast sizes of 16-32 mm, i.e. coarse lapilli (White and Houghton 2006) have been considered for textural purposes. Such clasts were considered to be large enough to be easily sampled and studied, while being fully representative of the density variation of the majority of erupted pyroclasts and unaffected by significant post-fragmentation phenomena (Houghton and Wilson 1989). These requirements are not always met. In basaltic magma, post-fragmentation effects can be a complication even for these sizes (e.g., Cashman et al. 1994; Szramek et al. 2006; Costantini et al. 2010; Gurioli et al. 2008; Pioli et al. 2014; Pistolesi et al. 2008; 2011; Stovall et al. 2011; 2012). In these cases, the challenge is to identify, quantify and remove post-fragmentation effects in order to isolate textures preserved across the fragmentation zone. For example, the original shapes of vesicles may be reconstructed by de-coalescencing large vesicles using the presence of broken, or partially retracted, glassy septa.

However, if we study an ash-dominated or a bomb-dominated event, particle-texture analyses must be performed on the fine or coarse juvenile fragments, respectively. Ash size particles (<2 mm) have been investigated recently in terms of vesicle and crystal size distributions (Taddeucci et al. 2002, 2004; Cioni et al. 2008; D'Oriano et al. 2011a, b; Miwa et al. 2009; 2013; Miwa and Toramaro 2013; Proussevitch et al. 2011; Genareau et al. 2012; 2013; Colucci et al. 2013, Schipper et al. 2013), and an extensive work has been done in the last 40 years in characterizing ash morphology and deposit componentry (Table 1). For the ash fraction, post-fragmentation expansion can be excluded (e.g., Proussevitch et al. 2011; Genareau et al. 2012; 2013; Colucci et al. 2013). Consequently, analyses allow comparison between morphological and textural features of clasts sampled in proximal and distal areas. Ash particles can record most of the information related to magma ascent dynamics (e.g., decompression-driven microlite crystallization) and fragmentation (Cioni et al. 2008;

D'Oriano et al. 2005; D'Oriano et al. 2011a, b; Proussevitch et al. 2011; Genareau et al. 2012; 2013; Colucci et al. 2013). Advantages of studying ash are that it can also be statistically more representative of the variability of the magma properties and is less affected by density-driven settling within the plume. However, ash fragments record only small-scale vesicularity. The integration of observations made on the external shapes of clasts may give information about the presence and importance of a coarser vesicularity which drives magma fragmentation (e.g., Proussevitch et al. 2011; Genareau et al. 2012; 2013; Colucci et al. 2013). However, they cannot provide complete information about the abundance and size of the full vesicle population, if the magma included bubbles larger than the ash particles. Furthermore, ash particles are not suitable for permeability studies, as they are often smaller than the bubbles forming the permeability network. However, the presence of coalesced vesicles in a preferred direction, and an abundance of ash clasts with an elongate shape, have been interpreted as an indication of the development of a permeable bubble network (D'Oriano et al. 2011a).

Bombs may provide a plethora of information regarding pre-eruptive degassing and ascent rate (e.g. Hoblitt and Harmon 1993; Wright et al. 2007), timing and degree of thermal interaction of magma with wall-rock material prior to ejection (Rosseel et al. 2006; Sottili et al. 2009; 2010), post-fragmentation changes due to bubble growth, coalescence or shape changes (e.g. Herd and Pinkerton 1997, Shin et al. 2005) and mingling between stagnant and fresh magma (Gurioli et al. 2014; Leduc et al. 2015).

(ii) Bulk measurements of particle characteristics

The fastest and most straightforward textural measurement of individual pyroclasts is density (vesicularity), which provides basic information on processes related to gas exsolution and escape (Houghton and Wilson 1989). The densities of lapilli and small bombs can be determined by comparing their weights in water and air following the Archimedes principle. Clasts can be made impermeable with silicone waterproofing spray, by immersion in cellulose acetate, or by using Parafilm^{TM} wax. This technique is fairly rapid and yields large arrays of data with a reproducibility within 10-30 kg m^{-3} and accuracy within 30 kg m^{-3} (Barker et al. 2012). Quicker, more timely and precise, density measurements can now be performed using a commercial envelope-density measurement device (http://www.micromeritics.com/Product-Showcase/GeoPyc-1360-Envelope-Density-Analyzer.aspx). Following the same principles, a battery-powered device has been used to vacuum-seal pumice or scoria in plastic bags in the field (Kueppers et al. 2005).

For pyroclasts characterized by fine vesiculation (with largest vesicles smaller than 2-3 mm), the density can be measured with the glass-bead method (Nakamura et al. 2008) that allows the calculation of the density as well as the volume of an object of irregular size. For large bombs (from 15 to 40 cm in diameter), a "natural waterproofing" effect was exploited (Gurioli et al. 2013). Extensive tests showed that decimetric size bombs collected at Stromboli acquired a "natural waterproofing" from their quenched margins and thus could be weighed in water without waterproofing. This represents an easy, precise and fast strategy for large bombs.

The derived density distributions, coupled with external morphology variation, can be used as filters to select a few clasts, representative of the low, modal and high density values, from each subpopulation observed (e.g., Shea et al. 2010a). Selected clasts are then used for textural quantification.

Other bulk particle-texture measurements include vesicle connectivity, permeability (Klug and Cashman 1996; Klug et al. 2002; Formenti and Druitt 2003; Rust and Cashman 2004; and references in Table 1) and electrical conductivity (Le Pennec et al. 2001; Bernard et al. 2007; Wright et al. 2009; Wright and Cashman 2014). The connectivity measurements are mostly performed using gas-displacement helium pycnometers, and they deliver first-order information on the outgassing capacity (i.e., potential for gas loss) of the magma near fragmentation (Klug et al. 2002; Formenti and Druitt 2003; Giachetti et al. 2010; Shea et al. 2011; 2012). Permeability controls the rate at which magma outgases during decompression. Several methods exist for permeability measurements in volcanology. Rust and Cashman (2004) used a commercial permeameter to perform systematic steady-state gas-flow experiments using porous samples, and the relationship between flow rate and pressure gradient was determined. They also introduced the Forchheimer equation into volcanology, which is a modified form of Darcy's law that includes the inertial effect of gas flow, and specified the importance of this effect in volcanic degassing processes. Mueller et al. (2005) used gas-pressure decay with time after sudden decompression in a fragmentation bomb for the permeability measurements, without measuring gas-flow rate. A falling head permeameter developed by Burbié and Zinszner (1985) has also been used to measure the permeability of volcanic porous materials (Jouniaux et al. 2000; Bernard et al. 2007). Recently, a low-cost gas permeameter was developed (Takeuchi and Nakashima, 2005) and improved (Takeuchi et al., 2008), to measure permeability of natural samples and experimental products. Finally, electrical conductivity measures how well a material transports electric charge. Rocks, in general, are poor conductors, whereas ionic fluids are good conductors. Therefore a

measurement of conduction through fluid-saturated rocks provides information about the connected pore pathway through the sample. Although the influence of pathway tortuosity and pore shape on permeability is useful for numerical simulations on gas percolation, it has been the object of only a few studies (Table 1).

(iii) Comparison between 2D and 3D particle-texture measurements

Two different methods are currently available for extracting vesicle and crystal sizes, shapes and distributions in pyroclasts. The first is by conversion of 2D data from a planar surface (such as a thin section or photograph) to 3D data through stereology. The second method derives 3D data directly from X-ray tomographic reconstructions and visualization of clast textures without the need of stereological conversions (Song et al. 2001; Shin et al. 2005; Polacci et al. 2006b; 2008; 2009a, b; 2010; Degruyter et al. 2010b; Gualda et al. 2010; Giachetti et al. 2011; Baker et al. 2012), using computer software especially developed for geo-textural purposes (e.g. Ketcham and Carlson 2001; Ketcham 2005; Friese et al. 2013). Other 3D methods include serial sectioning (e.g. Bryon et al. 1995), serial focusing with optical microscope (Manga 1998), serial grinding (e.g., Marschallinger 1998a, b, c; Mock and Jerram 2005), and constructing digital elevation models of individual ash grains to calculate vesicle volume (Proussevitch et al. 2011). Two-D and 3D observations have different limitations and potential, and the two methods are becoming complementary, not competitive (e.g., Giachetti et al. 2011; Baker et al. 2011).

2D method

Standard procedures for the 2D method have been recently published for vesicles (Shea et al. 2010a) and crystals (Higgins 2000; 2006). Two-D techniques can yield high-quality data and account for both vesicle and crystal sizes in the sample and can be applied to particles ranging in size from bombs (e.g., Gurioli et al. 2014, Leduc et al. 2015) to ash (Miwa et al. 2009; 2013; Miwa and Toramaru 2013). These measurements are best used when there is a broad size distribution to be measured. The main limitation of the method is that is based on the assumption of spherical shape of the textural objects, following Sahagian and Proussevitch (1998). When this conversion is simply obtained by dividing the number of vesicles per unit area by the median value of diameter of each size class (Cheng and Lemlich 1983), no shape assumption is made. However, the 3D conversion is more precise when a shape is defined. Empirical corrections are commonly used for crystal analyses (Higgins 2000 and 2006), but

for vesicles, whose shapes are less uniform, they risk introducing systematic, uncontrolled errors in the data (Sahagian and Proussevitch 1998; Proussevitch et al. 2007a; 2007b).

3D method

X-ray-computed microtomography is the only available high-resolution, non-invasive 3D technique that allows reconstruction, visualization and processing of samples. Data acquisition is generally relatively straightforward, and several scales can be examined and combined, ranging from centimeters to <1 micron, depending on the resolution (Giachetti et al. 2011). In addition, the so-called 'local area' tomography technique (e.g., Lak et al. 2008) enables high resolutions to be attained, even with samples larger than the field of view of the camera. However, 3D quantification of textures can also be labor intensive, depending on the size of the volume that needs to be analyzed and on the textural parameters required. The results show the internal structures of samples, highlighting how objects and apertures are linked together. This information provides an excellent suite of data for studies of vesicle size, shape and distribution, collapse, deformation, coalescence, permeability, and tortuosity, as well as for determining crystal volume, size and distribution and visualizing crystal aggregates in 3D (Polacci et al. 2009a, b; 2012; Bai et al. 2010, 2011; Degruyter et al. 2010a, b; Zandomeneghi et al. 2010; Gualda 2010a, b; Baker et al. 2012; Castro et al. 2012; Okumura et al. 2013). Vesicles with complex shapes are easily identified, while in a 2D section they might be interpreted as two or more vesicles, thus biasing vesicle size distribution (VSD) and vesicle number density (N_v) (e.g. Giachetti et al. 2011). The 3D method is particularly effective for determining N_v if the study is focused on a specific size range; vesicle number densities over a wide range of sizes is achieved with nested studies in which a series of scans are done at different sizes and resolutions (e.g. Giachetti et al. 2011; Pardo et al. 2014b). However, the resolution of the reconstruction is still critical. Klug et al. (2002) showed that vesicle walls may be as thin as 0.1μm. To achieve this sort of spatial resolution using tomography requires very small samples. When the attained resolution is 5-15 μm, thin vesicle walls are not resolved.

There is currently no unique protocol for 3D measurements of different types of pyroclastic (or lava) samples; however the SYRMEP group of the Elettra Synchrotron Light Source (Trieste, Italy), together with researchers at McGill University of Montreal and INGV Pisa (M. Polacci), are developing protocols for volcanic samples of different vesicularities and crystallinities.

(iv) Crystal size distribution

Crystal size distribution (CSD) is a well-established tool for interpreting the physical processes and environmental variables that drive differentiation and crystallization in magma chambers and conduits (e.g., Marsh 1988; Cashman and Marsh 1988; Cashman 1992; Hammer et al. 1999; Cashman and McConnell 2005, Armienti 2008; also see references in Table 1). CSD, coupled with vesicle distribution data, yield deeper insights into the physical processes operating in the conduit (e.g., Gurioli et al. 2005; D'Oriano et al. 2005; Piochi et al. 2005; 2008; Noguchi et al. 2006; Giachetti et al. 2010; D'Oriano et al. 2011a; Vinkler et al. 2012). The CSD method has been well tested and widely applied (Table 1), so that it is now quite straightforward to quantify CSD (Higgins 2000; 2006; and references in Table 1).

However, we must keep in mind that crystals are commonly anisotropic, and therefore shape cannot be ignored. Most studies use the Higgins technique to account for shape. However, the Higgins method assumes that all crystals are the same shape. This is clearly not true, as small crystals are often more anisotropic than large crystals. Treating all crystals in the same way can introduce artifacts (see Castro et al. 2003). In addition, there are still resolution issues for microlites, as well as problems in both back-scattered electron (BSE) and cathode ray tube (CRT) analyses when the crystals have a density (Z number) near that of the glass. Several methods can be used to facilitate the extraction and quantification of crystals. CSDs of larger crystals (phenocrysts, antecrysts, etc.) can be measured from transmitted light microscopy images of thin sections and analyzed with digital image analysis to automate and hence speed up the quantification process (e.g., Armienti et al. 1994; Launeau et al. 1994; Lumbreras and Serrat 1996; Goodchild and Fueten 1998; Launeau and Cruden 1998; De Keyser 1999; Heilbronner 2000; Armienti and Tarquini 2002; Boorman et al. 2004). Tarquini and Favalli (2010) used a slide scanner to acquire input imagery in transmitted light from thin sections and GIS software to analyze the data.

Crystals can also be identified using a scanner and a polarizing filter placed at different angles (Pioli et al. 2014). Three pictures are then combined, and their correlation allows the individual grains to be classified by their characteristic orientation. To measure smaller crystals (microphenocrysts and microlites), a scanning electron microscope is commonly used in backscattered electron (BSE) mode (Cashman 1992; Hammer et al. 1999; Cashman and McConnell 2005; Nakamura 2006; Ishibashi and Sato 2007; Salisbury et al. 2008; Blundy and Cashman 2008; Wright et al. 2012). Development of rapid x-ray mapping techniques now allows CSD analysis of x-ray element maps, which provide information on crystal

compositions, textures (crystal size, orientation, shape) and modes of minerals (e.g., Muir et al. 2012; Leduc et al 2015). Another new technique uses an electron backscatter diffraction detector (EBSD) attached to the SEM to obtain crystal orientations, which can provide insights into shearing, accumulation and degassing processes (Prior 1999; Prior et al. 1999; Hammer et al. 2010). Chemical mapping is now routinely and widely used (e.g., Leduc et al. 2015). In contrast, EBSD is more difficult to use and interpreting the data is harder than the chemical maps. As described in the references cited, it produces a wealth of information on various minerals, although the monocline structure of the feldspar can be problematic.

Crystal size distribution can also be obtained directly in 3D via X-ray computed microtomography. Using this approach, it is possible to obtain the total crystal volume, as well as the crystal volume of each mineral phase present: crystallinity, crystal size and crystal shape (e.g., Zandomeneghi et al. 2010; Voltolini et al. 2011). Again, resolution can be a problem. First, crystals may span a large size range, which requires imaging at several different resolutions (e.g., Pamukcu et al. 2010; 2012). Additionally, as in BSE analysis, the compositional similarity between some crystal phases, such as alkali feldspars, and silicic matrix glass can make automated analysis challenging (e.g., Baker et al. 2012). However, excellent results can be obtained by working in phase-contrast tomographic mode (Polacci et al. 2010), and applying a procedure known as phase retrieval to the reconstructed sample volumes (Arzilli et al. 2013).

(v) Errors in particle-texture analyses

Uncertainties in textural analysis are due to several factors. Any textural parameter, such as porosity or crystal size, has intrinsic measurement errors. These are linked to the apparatus used and are generally easy to quantify using standards. A good practice, when a new method is introduced, is to assess its intrinsic error with synthetic samples of well-known particles, having textural components (e.g. crystals, vesicles/voids) with known size and distribution (e.g., see review of Rust and Cashman 2004 for permeability, and Baker et al. 2011 for 3D data from X-ray microtomography). Another type of uncertainty is linked to natural variability, which is generally approached by using the concept of Representative Elementary Volume (REV, Bear 1972). Parameters measured in small, neighboring, regions within a sample have a large variability. As the analyzed regions become larger, this variability decreases until a steady value is reached at the REV size. One complication is that the REV should be significantly smaller than the sample (not guaranteed for ash, or even lapilli,

409 particles), and that some parameters have an REV at the deposit scale, which means that many
410 clasts have to be analyzed. If the sample location is such that eruptive parameters were steady
411 during deposition, application of REV at the deposit scale allows analysis of magma at the
412 point of fragmentation in the conduit. Taking porosity as an example, one 2D SEM image will
413 yield one porosity measurement with a typically small (~1 %) intrinsic error due to
414 thresholding of the grayscale values that represent vesicles. Several 2D images of the same
415 sample taken at different locations and/or different resolutions (larger than the REV) typically
416 yield larger (~10 %) uncertainties that are caused by small-scale spatial heterogeneity. Finally,
417 if we assume that – or if we have a – very well sorted deposit, then the density distribution of
418 all clasts at that location indicates the variability of porosity at the conduit scale, which can be
419 quite large (e.g., Houghton and Wilson 1998). The situation is more complex with poorly
420 sorted deposits in which particles range from bombs through lapilli to ash.
421 Raw data in terms of size (area, long axis, short axis, perimeter) and orientation of crystals
422 and vesicles yield negligible intrinsic errors, because they are computed with programs on 2D
423 binary images with high resolution (>10^6 pixels). In this phase, the uncertainty is due to the
424 image clean-up process, which is generally unquantified (because it takes too long to have
425 four people complete the task independently and then take the average for every image).
426 The greatest source of intrinsic error here is thresholding, which is set by the operator
427 (Baker et al. 2011). When converting 2D data to a 3D projection, however, the error depends
428 on the stereological model used (i.e. particle shapes have to be assumed, Cashman 1988) and
429 is thus harder to estimate.
430 Most 2D textural parameters have well-established techniques and protocols to quantify
431 intrinsic errors, including:
432 • VSD (Toramaru 1990; Mangan et al. 1993; Klug and Cashman 1994; 1996; Klug
433 et al. 2002; Adams et al. 2006b; Shea et al. 2010a),
434 • CSD (Higgins 2006), fabric indicators (Launeau et al. 1990),
435 • vesicle shape (Moitra et al. 2013),
436 • clast shape (Marshall 1987; Capaccioni and Sarocchi 1996; Dellino and Liotino
437 2002; Riley et al. 2003; Ersoy et al. 2006).
438 However, conversion from 2D to 3D distributions introduces errors linked to stereological
439 assumptions. The Cheng and Lemlich (1983) method does not involve assumptions of object
440 shape, but it does not take into account a truncation effect (e.g. Pickering et al. 1995).
441 Truncation is related to the sensitivity of the measurement process; smaller objects are

increasingly difficult to detect. On the other hand, large-scale truncation occurs under several circumstances related to sample-size (volume and area) limitations. The Sahagian and Proussevitch (1998) conversion assumes spherical shapes and corrects for the cut effect (this being the effect induced by rarely cutting a spherical object through its exact center). Giachetti et al. (2011) found that N_v obtained by 2D and 3D methods for the same lapilli agreed within 15 %, and that VSD were also very similar. They recommended the Cheng and Lemlich (1983) method for 2D vesicle analysis, as the Sahagian and Proussevitch (1998) method may generate negative values for some size classes.

In terms of parameters that we can derive from textural analyses, decompression rate is probably one of the most important to quantify due to its implications for eruption dynamics. To achieve this, microlite shape, N_v and size distribution have been used in combination with experimental data for low-mass flux and effusive eruptions (Couch et al. 2003; Cashman and McConnell 2005; Szramek et al. 2006; Clarke et al. 2007; Martel 2012; Wright et al. 2012). Martel et al. (2006) consider this approach to be highly reliable, because different generations of microlites (nucleated pre-eruptively in the reservoir or syn-eruptively in the conduit) can be distinguished on the basis of chemical composition. Decompression rates deduced from N_v (e.g., Toramaru 2006), however, tend to be maximum estimates, because there could be more nucleation events during ascent that add to the signature left by decompression. Maximum decompression rates associated with the final, rapid, stages of ascent could be calculated directly from the smallest bubbles formed during the final fragmentation event (Giachetti et al. 2010; Shea et al. 2011; 2012). Another developing method is to use chemical gradients of volatiles in melt inclusions in crystal embayments to infer rise rates (Ferguson et al. 2013).

However, the relationships between bubble shape, nucleation, coalescence, deformation and/or fragmentation are not well established yet.

Quantification and sampling of pyroclastic deposits for the textural characterization of their components

(i) Preliminary field studies and sampling strategy

Field-based studies of pyroclastic deposits aim to relate both the whole-deposit characteristics (thickness and grain size) and the physical properties of the constituent particles to the eruption conditions. Particle-texture studies are time consuming, especially when they provide complete size distributions of the vesicle and crystal population. For these measurements, the

choice of a limited number of "representative" clasts selected for the analysis is critical, particularly when using these data to model eruption processes and their variability in time and space. Obtaining such clasts requires a cautious sampling strategy with well-defined scientific goals during field work. These studies are best performed only on well-documented deposits, supported by a robust stratigraphic reconstruction and correlation, as well as an accurate compositional stratigraphic framework. When not familiar with the deposit, a preliminary survey at different locations is useful to evaluate the significance of the outcrops used for detailed analysis. Well-defined sublayers (or units) should be identified in the deposit on the basis of clear, unequivocal lithologic and sedimentologic features and cross-correlated over the whole dispersal area of the deposit. Stratigraphic data are critical for placing each studied layer within an appropriate temporal framework within the stratigraphic sequence.

Pyroclasts can be collected after the eruption, from fall deposits of old (unobserved) or recent (observed) eruptions, for which sampling is done preferably within hours to days of the event (e.g., Gurioli et al. 2008; 2013). Sampling may also take place during eruptive activity, with samples collected using sampling device placed inside the fallout field. Three simple collection methods that can be applied to active fallout, as currently used, are: (1) the hand collection method involves collecting (and quenching) bombs or lapilli as they fall out of the plume by people standing in the active fallout field (e.g., Lautze and Houghton, 2007, 2008; Gurioli et al. 2014); (2) the "clean surface" strategy, whereby plastic sheets are laid out close to the vent, or a preexisting surface is cleaned before the eruption. In both cases the pyroclasts falling in a known area are collected (e.g., Rose et al. 2008; Andronico et al. 2009a; 2013a and b; Eychenne et al. 2012; Houghton et al. 2013, Harris et al. 2013b, Schipper et al. 2013); (3) the bucket strategy, in which a large number of buckets are distributed across a discrete area of fallout for a certain period of time (e.g., Yoshimoto et al. 2005; Swanson et al. 2009; Bustillos and Mothes 2010). When possible, the aims are to collect a sufficient number of samples to estimate the magnitude of the event through the mass load per unit area; and to obtain a sufficient number of clasts for chemical and textural characterization. Other promising methods are just coming on-line, such as automatic ash sampling collectors (e.g., Bernard 2013; Shimano et al. 2013, Marchetti et al. 2013).

(ii) Definition of essential, basic physical properties of the deposit to the study

Most particle and deposit texture studies aim at characterizing magma heterogeneity and ascent dynamics, and at understanding the fragmentation process, beginning with the size,

morphology and componentry of the particles (Table 1). Clasts selected for particle-texture analysisare usually sampled in a deposit at a single location (reference section). Lateral variability across the deposit is filtered by transport and sedimentation processes, which primarily depend on eruption intensity, along with related plume dynamics and other dynamic effects such as wind direction and velocity and rainfall. Therefore, clast properties can differ both in time (from the base to the top of a vertical sequence) and in space (from the main axis of dispersal to lateral outcrops at the edge of the fallout zone across the cloud, and from proximal to distal sites). Volcanic plumes (and clouds) are thus complex systems, the properties of which do not vary linearly with the main eruption parameters. They are also affected by external variables, such as wind direction and velocity. The external variables add additional complexity to the clast-type distribution. For this reason, the deposit should be preliminarily characterized at least in terms of stratigraphy, dispersal, thickness variation and volume before more detailed study is initiated (e.g., Fisher and Schmincke 1984; Cas and Wright 1987; Thordarson et al. 2009; Cioni et al. 2011). Estimation of plume height, eruption duration, volume and magma eruption rate can then also be derived for past eruptions from such analyses (e.g., Carey and Sparks 1986; Pyle 1989; Fierstein and Nathenson 1992; Sparks et al. 1997; Bonadonna et al. 1998; Freundt and Rosi 1998; Bonadonna and Costa 2012; Fagents et al. 2013).

(iii) Selecting the outcrop

There are three basic criteria for sample outcrop selection. First: minimize the effect of wind dispersal. Outcrops located along the main dispersal axis are preferred to lateral exposures, unless the effect of wind is the target of study. If wind direction or eruption intensity changes during different phases of the same eruption, it is more appropriate to sample each tephra layer at different ‘equivalent’ locations rather than to collect all samples at a single type outcrop. If sampling is restricted to a single location, the inferred dispersal pattern and distance from the main dispersal axis of each layer should be noted and taken into account when analyzing clast variability among different layers.

A second criterion for selecting the outcrop is that clear textural variations among the juvenile clasts, in terms of color, general morphology, vesicularity, vesicle shape, and crystallinity should be evaluated in the preliminary field survey, so that any lateral and vertical variability within the deposit is already defined following field reconnaissance. This

543 ensures that, when clast types are chosen in the laboratory, the main textural types are easily
544 identified and separated.
545 The third criterion for outcrop selection, if one of the goals of the study is quantification
546 of the proportion of distinct textural clast types, is to remember that sedimentation from the
547 volcanic plume is affected by clast density, shape and size (Bonadonna et al. 1998; Pfeiffer et
548 al. 2005; Barsotti et al. 2008; Eychenne et al. 2013, and references therein). This is especially
549 relevant when a single explosion produces a juvenile population with a wide range of textural
550 and other physical features: their relative proportions within the deposit can vary laterally in
551 the deposit as well as with distance from the vent. Thus, at any single site, the sample is not
552 necessarily representative of the abundance within the eruption mixture. This is especially
553 true in the case of small plumes and mid-intensity eruptions (e.g., Rose et al. 2008; Cioni et
554 al. 2008; 2011; D'Oriano et al. 2011a; Andronico et al. 2013a and references therein). While
555 the textural features of the different clast types can be studied at a single outcrop, the relative
556 proportions between clast types need to be determined across the whole deposit by integrating
557 componentry data on samples collected at outcrops at differing azimuths and distances from
558 the source.
559
560 (iv) Sampling
561
562 After identification of the outcrops where the deposit shows the best and most complete
563 exposure, a suitable approach is random collection of a statistically relevant number of clasts
564 from a single layer. Several techniques can be used, ranging from sieving in the field to find
565 the dominant clast size (for coarse clasts), or sampling the bulk deposit for later clast selection
566 in the laboratory (for small clasts). In the case of fine-grained deposits, it can be useful to
567 apply sampling techniques that preserve structural and textural characteristics of the whole
568 deposit. Samples can be retrieved using tubes or boxes manually pressed into the deposits, or
569 carfully carved out and surround-wrapped deposit blocks. In situ and/or laboratory
570 impregnation techniques of deposits exist for a broad range of grain sizes and compositions
571 (Bouma 1969), some of which are applicable to fragile or loose volcanic deposits (e.g. Fiske
572 et al 2009). The applicability of such techniques to fine-to-medium grained volcanic deposits
573 should be tested, since they would allow both 2D (e.g., X-ray radiography and thin section
574 analysis) and 3D analysis (X-ray tomography and anisotropy of magnetic susceptibility) to be
575 applied to deposits, rather than single pyroclasts; these, techniques are frequently used for
576 hard rocks (e.g., Lanza and Meloni 2006).

577 The number of samples should be defined depending on the purpose of the study.
578 Fixing the number of samples per stratigraphic layer based on the layer characteristics (e.g.,
579 extent of zoning/fluctuations in grain-size, componentry, etc.) for characterizing eruption
580 dynamics, or focusing on the layer thickness for conduit dynamic characterizations, are two
581 examples of such pre-selection decisions. Before selecting clasts, basic grain-size studies
582 (when the bulk deposit is collected) on each sampled layer (median and sorting of grain-size
583 distribution) and componentry analysis should be carried out to ensure effective sub-sampling
584 for textural studies. Following White and Houghton (2006) componentry analysis is the
585 subdivision of the sample into three broad components: juvenile, non-juvenile particles and
586 composite clasts. The juvenile components are vesicular or dense fragments, as well as
587 crystals, that represent the primary magma involved in the eruption; non-juvenile material
588 includes accessory and accidental fragments, as well as crystals, that predate the eruption
589 from which they are deposited. Finally, the composite clasts are mechanical mixtures of
590 juvenile and non-juvenile (and/or recycled juvenile) clasts. More-detailed componentry can
591 subdivide the juvenile and non-juvenile materials into subpopulations that have important
592 dynamic meanings (e.g., Eychenne et al. 2015).
593 Finally, after choosing the size intervals of the clasts for physical and textural
594 measurements (i.e., bulk and solid density, vesicularity, microtextures, permeability), it is
595 useful to compare the grain-size distribution of each interval with the total grain-size
596 distribution of the sampled layers, especially when the grain-size distribution is highly
597 variable within the sampled stratigraphy. This strategy allows checking of sample
598 representativeness. For example, sampling may be from (i) bimodal or complex multimodal
599 distributions, or (ii) anomalous, poorly sorted deposits. In the second case, sampling should
600 avoid features that can be indicative of contamination from other sources, such as ballistic
601 components, elutriated ash from pyroclastic density currents or from reworking (e.g., Fierstein
602 et al. 1997, Eychenne et al. 2012). It is useful, whenever possible, to show variance, or
603 invariance, of the textural features by comparing data collected in the selected size class with
604 textural data for different size classes. This should, at least, be carried out for a few selected
605 samples.
606
607 **How to link petrological, geochemistry and textural quantifications**
608
609 (1) Initial parameters and conduit processes
610

611 Geochemical and petrological analysis of pyroclastic products can constrain the initial
612 conditions in the shallow crustal holding chamber through to the surface via the conduit
613 system (Fig. 1). In transit through this system, the textural features are imprinted on the
614 pyroclasts quenched upon eruption. The geochemical and petrologic analysis can help:

615 • Define pre-eruptive P-T storage conditions from mineral-melt equilibria or
616 disequilibria (e.g., Rutherford et al. 1985; Scaillet and Evans 1999; Pichavant et al.
617 2002; Blundy and Cashman 2008; Schipper et al. 2010b);
618 • Assess initial viscosity, temperature, melt composition and volatile budget, including
619 input of gases from deeper sources (e.g., Wallace 2001; Blundy and Cashman 2008;
620 Métrich et al. 2010);
621 • Define the evolution of volatile contents (specifically CI, F, S, H_2O, CO_2) using
622 electron probe, ion probe (SIMS), Raman and FTIR in melt inclusions and host
623 minerals, while combining results with vesiculation studies and gas release
624 measurements (e.g., Wallace 2005; Métrich and Wallace 2008, Schipper et al. 2010c).
625 In such a way we can determine whether the magma was saturated, over-saturated or
626 under-saturated at a certain depth, and how these conditions affect vesiculation in the
627 conduit (e.g., Anderson 1991; Hurwitz and Navon 1994; Dixon 1997; Roggensack et
628 al. 1997; Schipper et al. 2012);
629 • Measure residual volatiles in glasses and bulk-rock samples to reveal how degassed
630 the magma is (Newman et al. 1988; Villemant and Boudon 1998; Shea et al. 2014);
631 • Provide variable diffusion of stable elements (^{6}Li, ^{7}Li, H/D, ^{10}B, ^{11}B) or radiogenic
632 isotopes (^{210}Pb-^{226}Ra), which are used as tracers for melt degassing and interaction
633 with hydrothermal fluids (e.g., Berlo et al. 2004; Kent et al. 2007; Humphreys et al.
634 2008b; Schiavi et al. 2010; Berlo and Turner 2010; Vlastélic et al. 2011);
635 • Measure mineral diffusion profiles and derive pre-eruptive residence times, ascent
636 rates and cooling rates (e.g., Kahl et al. 2011);
637 • Provide crystal shapes, zoning schemes, and dissolution stages, while determining
638 which magmatic process and physical parameters control crystal shape/zoning (e.g.,
639 Hammer and Rutherford 2002; Rutherford and Devine 2003; Blundy et al. 2006; Costa
640 et al. 2008; Streck 2008);

641 In addition, laboratory petrological investigations can provide:

- Experimental observations on phase equilibria (mineral-melt-vapor), crystallization paths and liquid line of descent (e.g., Hammer and Rutherford 2002; Couch et al. 2003; Blundy et al. 2006; Hammer 2008);
- Calibration of decompression rates. While this has been carried out for rhyolitic systems (e.g., Mourtada-Bonnefoi and Laporte 2002, 2004; Mangan and Sisson 2005; Gardner 2007; Cichy et al. 2011; Cluzel et al. 2008) and phonolitic systems (e.g., Larsen 2008; Shea et al. 2010b), there are ongoing studies on basaltic systems (Bai et al. 2008; Lesne et al. 2011; Pichavant et al. 2013);
- Diffusion coefficients of relevant chemical elements, including volatiles, to improve kinetic modeling (Dohmen et al. 2007; Chakraborty 2008);
- Relationships between crystal morphologies, cooling rates and degree of undercooling (e.g., growth of crystals with hopper and swallow tail shapes experiencing rapid late-stage crystallization; Faure et al. 2003, 2007);
- Surface flux of volatiles (i.e. what leaves the system; see reviews by Fischer 2008; Pyle and Mather 2009) compared with melt inclusion data (i.e. what is in the system initially; e.g., Le Voyer et al. 2010; Rose-Koga et al. 2012; Schiavi et al. 2012).

2) Where geochemistry can help textural study

Measurements of volatile contents in quenched, phenocryst-hosted melt inclusions provide estimates of initial (shallow crustal) values (e.g., Kent 2008). These are minimum estimates, because H_2O can leak from melt inclusions during ascent by intracrystalline diffusion as the far-field environment of the crystal evolves (Chen et al. 2011, 2013). Melt inclusion volatile contents can be inverted to equivalent saturation pressures using multi-species (e.g., H_2O-CO_2; H_2O-Cl) solubility laws (using, for example, VOLATILCALC, Newman and Lowenstern 2002; MELTS, Ghiorso and Sack 1995; Asimow and Ghiorso 1998). These, in turn, can be used to calculate total pressures (and hence depth) by assuming volatile saturation, or minimum pressures if the sample is under-saturated in volatiles. Progressive closure of melt inclusion networks in growing phenocrysts can result in zone-dependent melt inclusion volatile contents that record the evolution of pressure conditions as magmas migrate from depth (Blundy and Cashman 2008, and references therein). Combining major element and volatile compositions of the melt with phenocryst contents allows calculation of initial magma physical properties (viscosity, density, surface tension, and others). Derivations of

675 such parameters are necessary for modeling magma ascent, vesiculation and groundmass
676 crystallization.
677 Pre-ascent storage conditions can also be inferred from phase-equilibria studies of natural
678 compositions. Comparison of natural and experimental phase abundances and compositions,
679 combined with constraints of volatile content (from melt inclusions) and temperature (from
680 e.g., Fe-Ti oxides) allows estimation of total pressure if the degree of volatile saturation is
681 established through use of mixed-volatile experiments (Pichavant et al. 2007; Cadoux et al.
682 2014).
683 Residual volatile content (e.g., H_2O, CO_2, SO_2, Cl, F) measured in the glass or directly
684 from gases emitted at the vent can be correlated with textures (e.g., Piochi et al. 2005; 2008;
685 Schipper et al. 2010a; Balcone-Boissard et al. 2011, 2012; Shea et al. 2012, 2014; Burton et
686 al. 2007; Polacci et al. 2009b; Miwa and Toramaru 2013). The residual volatile contents can
687 also be compared with pre-eruptive volatile contents obtained from melt inclusion to evaluate
688 both the extent and efficiency of syn-eruptive degassing (e.g., Shimano and Nakada 2006;
689 Noguchi et al. 2006, Métrich et al. 2001; 2010). Residual water content or Cl content (when
690 Cl partitions into a H_2O vapor phase, so that it can thus be used as an indicator of degassing
691 processes; Balcone-Boissard et al. 2010) is typically plotted against V_g/V_l, where V_g is the
692 volume of vesicles corrected for phenocrysts and V_l is the volume of melt and microlites
693 (Villemant and Boudon 1998, Balcone-Boissard et al. 2011, 2012). An important issue is to
694 assess the extent of post-eruption hydration. Recently, thermal gravimetric studies have
695 proved to be quite effective in allowing this correction based on oxygen or hydrogen isotopic
696 compositions (e.g., Giachetti and Gonnerman 2013; Shea et al. 2014). Studies of hydrogen
697 isotopes, correlated with SEM glass textures, permit distinction of magmatic water from
698 meteoric water generated by re-hydratation (Kyser and O'Neil 1984). Hydration can also be
699 assessed from the ratio of water species (molecular H_2O vs. OH) in residual glass, as
700 determined by FTIR data or Raman analyses (Hammer et al. 1999; Le Losq et al. 2012).
701 Ascent and decompression in the conduit can result in chemical changes that can be
702 quantified by a range of microbeam analytical techniques (e.g., EPMA, LA-ICPMS, FTIR, μ-
703 Raman). As the pressure drops, H_2O will migrate out of melt inclusions and crystals (Le
704 Voyer et al 2010; Hamada et al 2010), and light elements (Li, B) will try to re-establish
705 equilibrium between crystals, host melt and any vapor or brine phase present (Berlo et al.
706 2004). At the same time, H_2O and CO_2 migrating out of melt inclusions will become apparent
707 as re-entrant tubes at the edges of crystals (Liu et al. 2007; Humphreys et al. 2008a). Each of
708 these processes will establish diffusive gradients frozen into the pyroclast that can be

709 measured and modelled using experimentally determined kinetic laws to infer decompression
710 rates during ascent (e.g. Gonnermann and Manga 2013). These decompression rates can then
711 be compared with values derived from other approaches, including those based on analyses of
712 microlite sizes and shapes, vesicle number densities, and hornblende-breakdown reactions
713 (e.g., Martel 2012; Cluzel et al. 2008; Giachetti et al 2010; Shea et al. 2011).
714
715 3) Contentious points
716
717 Care needs to be taken when converting decompression rate to magma ascent rate, and
718 especially when comparing decompression rates obtained using different methods. Pressure
719 gradients in conduits are highly nonlinear due to the strong effect of dissolved H_2O on magma
720 viscosity, particularly at low H_2O contents (Gonnermann and Manga 2013). Moreover,
721 different processes will likely record different decompression rates, according to the time
722 available for the process to take place. For example, microlite growth is relatively slow, so
723 that microlite size and shape distributions are likely to record an average decompression rate
724 during ascent (Martel 2012). Bubble nucleation and growth, on the other hand, can occur very
725 rapidly, so that N_v may record just the peak decompression rate immediately beneath the
726 fragmentation zone (Cluzel et al. 2008; Giachetti et al 2010). Comparison of rate calculations
727 from different methods therefore requires caution. However, integration of decompression
728 rates as obtained from different textural and chemical characterizations, when combined with
729 mass eruption rate estimation from deposit analysis or direct observations, can provide
730 quantitative insights into the processes involved in magma ascent from the deep source to the
731 surface.
732 Another outstanding issue is the role of dense clasts. That is, did they originate (i) from
733 magma quenched at depth prior vesiculation, (ii) by vesicle collapse in an originally vesicular
734 clast, (iii) from volatile-poor magma or from reciclying? It is important to provide a correct
735 interpretation, because the three conclusions relate to very different mechanisms. In several
736 eruptions it has been found that the densest clasts were depleted in water through syneruptive
737 bubble collapse and coalescence (Rust and Cashman 2007; Piochi et al. 2008, Shea et al.
738 2014). In Plinian eruptions at Vesuvius (Pompeii and Avellino), the densest clasts have been
739 interpreted as magma that lost water during transition from closed-to open-system degassing
740 (Balcone-Boissard et al. 2011; 2012). Water depletion can also result from syn-eruptive
741 processes, such as clast recycling at magmatic temperature (Gurioli et al. 2014) and intrinsic
742 magmatic redox conditions, as shown by the experiments of D'Oriano et al. (2012). No study

743 has yet have demonstrated that dense clasts retain all of their original gas and were quenched
744 at great pressure.
745 Another key question is whether the measured compositions (including volatile content)
746 of bulk rock, glass, or minerals represent equilibrium or disequilibrium processes, and if
747 equilibrium or disequilibrium conditions pertain to local subsystems or to the whole magmatic
748 body under investigation (see for example Pichavant et al. 2007). Chemical species with
749 different diffusivities, for example, record equilibrium or non-equilibrium conditions in the
750 same sample (e.g. De Campos et al. 2008; Schipper et al. 2012). Equilibrium kinetics is also
751 composition-dependent, because it is dictated in part by melt viscosity which is itself related
752 to viscosity. This issue will generally affect silicic to intermediate magmas more than basaltic
753 magmas. However, we note that even for basaltic systems crystal-fluid-bubble magma
754 mixtures can achieve apparent viscosities that range over six orders of magnitude, up to 10^6
755 Pa s (e.g., Gurioli et al. 2014), depending on the degree of cooling, degassing and
756 crystallization. Such rheological variation even within a single composition, and its effect on
757 eruption mechanisms, deserves increased attention.
758
759 **How to link the geophysical data with pyroclast textural quantification**
760
761 A wide array of remote sensing and geophysical approaches can be used to parameterize an
762 explosive event, both within and outside the conduit (Fig. 1). Geophysical signals are
763 generated by fluid and gas flow in the magma-filled part of the conduit and during
764 fragmentation. Magma-gas ascent dynamics and conduit conditions extracted from
765 geophysical data for this part of the system are particularly difficult to validate because the
766 system cannot be directly observed. They are thus effectively "invisible" to direct observation.
767 Measurements outside the conduit can be made of the emitted mixture of gas and particles as
768 it (i) exits the vent, (ii) ascends above the vent as a plume, and then (iii) drifts away from the
769 vent as the cloud. Models and dynamic parameters extracted for geophysical and remote
770 sensing data outside the conduit are a little easier to validate because they can be directly
771 observed.
772 The invisible part of the system is the realm of studies using seismic, pressure
773 (infrasonic), and deformation data. All three data sets have long been shown capable of
774 detecting the geophysical signature of explosive events spanning weakly explosive Hawaiian-
775 to-Strombolian through Plinian events. Seismic data sets are available, for example, for gas-
776 pistoning events, puffing, fountains, and strombolian eruptions at mafic systems (e.g.,

777 Goldstein and Chouet 1994; Ripepe et al. 1996; Sciotto et al. 2011; Ripepe and Braun 1994),
778 as well as for events that generate somewhat larger plumes during silicic eruptions, as at
779 Santiaguito, Soufriere Hills, and Redoubt. Associated pressure impulses (typically recorded
780 by infrasound and barometers) have long been recorded for such energetic events, famous
781 examples including the pressure response to the 1883 eruption of Krakatoa and the 1967
782 caldera-forming eruption of Fernandina (Simkin and Howard 1970). Magma-gas ascent has
783 also been shown to generate rapid, but recordable, deformation signals detected by tiltmeters
784 (Aoyama and Oshima 2008; Genco and Ripepe 2010; Iguchi et al. 2008; Zobin et al 2007).
785 Velocities, masses and size distributions of particles leaving the vent have typically been
786 measured by visible and thermal video (e.g., Chouet et al. 1974; Ripepe et al. 1993; Harris et
787 al. 2012; Delle Donne and Ripepe 2012; Taddeucci et al. 2012; Bombrun et al. 2014; Gaudin
788 et al., 2014a, b) and Doppler radar (e.g., Dubosclard et al 1999; Hort and Seyfried 1998; Vöge
789 et al 2005; Gouhier and Donnadieu 2008; 2011; Gerst et al 2013). Infrasonic array methods
790 are also available to locate the emission in x,y space (Ripepe and Marchetti 2002). Plume
791 front velocities, density and entrainment rates have also been successfully tracked using
792 visible and thermal cameras, as well as radiometers, for a few stronger, ash-rich, buoyant
793 plumes at Stromboli, Santiaguito and Eyjafjallajökull (Patrick 2007; Sahetapy-Engel and
794 Harris 2009; Bjornsson et al. 2013; Valade et al. 2014); See Chapter 9 of Harris (2013) for
795 review.
796 Satellite remote sensing has long been used to track and measure properties of the
797 eruption cloud as it drifts and disperses. These data are available for all cloud sizes, from
798 those associated with small Strombolian and fountaining events (e.g., Heiken and Pitts 1975;
799 Dehn et al. 2000; 2002) to sub-Plinian and Plinian events (e.g., Holasek and Self 1995;
800 Koyaguchi and Tokuno 1993; Holasek et al. 1996). Cloud dispersion dynamics are especially
801 well revealed by geostationary satellite data with nominal imaging of one image every 15
802 minutes and higher. Basic cloud properties that can be measured by satellite data include
803 cloud dimensions, drift velocity and height (e.g., Robock and Matson 1982; Denniss et al.
804 1998; Aloisi et al. 2002; Zakšek et al 2013). Prata (1989) and Wen and Rose (1994)
805 introduced a method to potentially extract particle size distribution and mass from “split
806 window” (10-12 μm) thermal data. While specially modified ground-based thermal cameras
807 were adapted to extract ash particle size and plume mass (Prata and Bernardo 2009), newly
808 available technology such as LiDAR and PLUDIX were shown of value in detecting, tracking
809 and measuring fine particles in the Eyjafjallajökull cloud (e.g., Bonadonna et al. 2011).
810 Disdrometers and ash collectors, however, currently show greater potential for measuring

811 particle size and terminal velocity (Marchetti et al. 2013; Shimano et al. 2013) than PLUDIX,
812 which was designed more for meteorological applications (Caracciolo et al. 2006; Prodi et al.
813 2011).

814 For the gas content of the cloud, satellite-based sensors such as TOMS, AIRS, OMI,
815 MODIS, GOME and IASI have been used to obtain the SO_2 content in the far field, once the
816 gas cloud has decoupled from the ash cloud (e.g., Krueger et al. 1990; Carn et al. 2003; 2005;
817 Watson et al. 2004; Yang et al. 2007; Thomas et al. 2011; Rix et al. 2012; Walker et al. 2012).
818 Ground-based sensors, such as COSPEC, FLYSPEC and DOAS (e.g., Caltabiano et al. 1994;
819 Horton et al. 2005; Oppenheimer et al. 2011), have been used to measure SO_2 fluxes relatively
820 close to the source; see Williams-Jones et al (2008) for full review. These approaches have
821 been recently supplemented by SO_2 camera systems, which allow 2D images of SO_2
822 concentrations to be collected at ~1 Hz rates (Mori and Burton 2006). Such studies have,
823 though, tended to focus on passive degassing and gas-puffing systems, because the presence
824 of ash interferes with UV-light transmission on which the technique relies, making
825 measurements problematic. Recently, SO_2 cameras have been used to measure the gas masses
826 and fluxes involved in discrete explosive events (Mori and Burton 2009; Holland et al 2011;
827 Barnie et al. 2014).

828 However, none of these remote sensing techniques directly collects or makes contact with
829 the magma or particles they measure. Thus the need exists for quality ground-truth data to
830 validate particle velocities and sizes extracted from what is, basically, an electronic response,
831 as well as to test the assumptions and models used to convert received "power" to a more
832 meaningful and useful parameter (such as mass). At the same time, any single data set can be
833 inverted to support a conduit or plume dynamic model; but results need to fall within
834 constraints provided by ground-truth data. In this case, ground truth is provided by analyses of
835 the magma and particles themselves to extract parameters such as magma temperature,
836 chemistry, density, crystallinity and vesicle content, as well as vesicle shape and size and
837 particle density, size, shape and roughness. Magma ascent, explosion-source and
838 fragmentation models based on geophysical data likewise need to be consistent with
839 independent measurements made for physical volcanology for the same processes if they are
840 to be valid. We explore below these needs, mostly focusing on weakly explosive, basaltic
841 cases, the usual targets because they provide a reliable and easy-to-measure source for testing
842 new technology, methods and algorithms for ground-based geophysical enquiry.
843

844 *The basic need: Realistic assumptions and validation*

The basic response of a remote sensing instrument is a voltage which, through calibration, can be converted at higher level physical value, such as spectral radiant intensity or power. The conversion of this value to higher level and more volcanologically useful parameters (such as particle-size distribution, mass flux or plume density) requires an increasingly complex system of assumption stacking. Thus, to adequately reduce geophysical data, a number of input parameters are required and many assumptions need to be made, all of which can be provided by the physical volcanological community. Data sets from this community, especially if provided simultaneously with geophysical data collection during an active event, or provided as a library typical of that event, can also be used to "ground truth" or check the precision and reality of the geophysically applied input or generated output.

Seismic signals that accompany explosions are primarily short period (SP; high frequency > 1 Hz) signals which are typically termed "explosion quakes". These usually have high amplitudes and mostly include frequencies up to a few hertz, with a possible higher frequency acoustic phase (McNutt 1986, Mori et al. 1989, Braun and Ripepe, 1993). Below these frequencies, short period (SP) signals are often hidden by very-long period (VLP) components with much lower amplitudes (Neuberg et al. 1994; Kaneshima et al. 1996). In-spite of an enormous amount of work, it remains unclear as to how we can explain the VLP seismic component, which itself is only one part of the seismic signal. It also remains unclear as to whether, and/or how, SP and VLP components are related to the magnitude and intensity of an explosion, although attempts have been made using tremor (Brodsky et al. 1999; Nishimura and McNutt 2008; Prejean and Brodsky 2011). Clearly, better coupling with the physical volcanology community could help narrow down much uncertainty and allow progress towards better models to untangle the seismic signal associated with discrete explosive events.

Delay times in the arrival of seismic, infrasonic and thermal signals have been commonly used to assess the depth at which various physical processes occur in explosive basaltic systems (e.g., Ripepe and Braun 1994; Ripepe et al. 2001; 2002; Harris and Ripepe 2007). However, the sound speed in the conduit needs to be assumed if, for example, the thermal-infrasound delay is to be used to obtain the fragmentation depth. This will vary strongly with conditions in the empty portion of the conduit, including mixture density, gas-to-particle ratio, and temperature of the mixture through which the sound is propagating. Thus we need to know these variables if we are to provide a realistic sound speed value and hence infer a plausible depth. We thus need to constrain two fundamental parameters to strengthen geophysical modelling of the shallow explosion mechanism and depth. First, the magma crystal and bubble content (as well as size, shape and distribution), plus fluid chemistry and

879 temperature, are needed to define magma rheology properties and bubble ascent dynamics.
880 Second, the exact proportions and character of the mixture of gas and particles that ascends
881 the final section of the conduit to exit the vent and feed the emission must be known.

882 Velocities, mass fluxes and particle size distributions (PSDs) for lapilli through bomb-size
883 particles have been derived from high spatial and temporal resolution video data obtained
884 using both near-infrared and thermal cameras (Chouet et al. 1974; Ripepe et al. 1993; Harris
885 et al. 2012; Delle Donne and Ripepe 2012; Bombrun et al. 2014).

886 Generally, these studies have focused on Stromboli. For such camera data, the lower limit
887 of a particle size that can be extracted is limited by pixel size. This is typically about one
888 centimeter in dimension, depending on the detector's instantaneous field of view and distance
889 to the target (Harris 2013). A pixel-mixture model can be applied to obtain the size of a sub-
890 pixel particle, but it needs to assume a temperature for the particle and then uses the pixel-
891 integrated temperature to solve for the pixel portion occupied by that particle (Harris et al.
892 2013a). Symmetry then needs to be assumed to convert from particle area to particle volume,
893 and a density needs to be assumed to derive particle mass (Bombrun et al. 2014). For ash-rich
894 plumes, methods have been applied to extract total plume mass and air entrainment properties
895 from ascent dynamics of buoyant thermals (Wilson and Self 1980; Patrick 2007; Valade et al.
896 2014). However, all methods need particle shape, particle density, plume density and/or size
897 distribution data to: (i) determine whether the input assumptions are valid; and (ii) ground
898 truth the remote-sensing-data-derived size and mass data (Harris et al. 2013a and b). The
899 advantage is, if a validated method can be developed, particle size distribution, mass and mass
900 flux data for the plume leaving the vent can potentially be provided multiple times per second
901 using camera data (e.g., Taddeucci et al. 2012; Bombrun et al. 2014).

902 Deducing the erupted mass from Doppler radar data requires the assumption of a particle
903 size distribution for the eruption. Because this distribution is unknown, an average particle
904 size can be constrained from the Doppler radar measurement, typically using the eruption
905 velocities themselves deduced from either terminal fall velocities (Hort et al 2003) or by
906 discriminating between lapilli (larger than a few millimeters or 1 cm, depending on the radar
907 wavelength) and fine ash particles (<1 mm) using their temporal velocity evolution (Valade
908 and Donnadieu 2011). Both methods can be used to obtain an estimate for the erupted mass of
909 ballistics. We thus need to know whether the constrained average particle size can be used for
910 mass calculation, whether the assumption is a good approximation, and what the difference
911 between the derived value and true value is.

912 The radar is able to measure particles of all sizes, provided enough particles are available
913 to return a signal. The relationship between particle size and number of particles required for
914 a signal that exceeds the noise level is not linear, however. It also depends on the radar
915 wavelength and the distance between the radar and target. The smaller the radar wavelength,
916 and/or the smaller the distance between the radar and target, the smaller the number of fine
917 particles needed for a return signal. For particles <1 mm, halving the particle size increases
918 the number of required particles by a factor of 64. Doubling the size of particles to >1 cm
919 means that only ¼ of the number of particles is needed to return the same signal amplitude. In
920 addition, radar can measure at points (gates) across the entire plume thickness. Currently,
921 radar's best role is to provide radial velocity measurements, with well-stated limits as to the
922 particle size to which these data relate, through the entire plume thickness.
923
924 *Questions, points and issues*
925 The main question from the geophysical community to the textural community is: "*What*
926 *does the magma look like at the point of fragmentation?*" Geophysical analysts need to know
927 everything possible about the fragments physically in order to reduce and model the data
928 correctly. To help with this, we concluded that:
929 - Measurements of basic geophysical parameters (such as seismic energy, acoustic
930 energy, energy partitioning, spectral radiance, and radar power) are the most
931 straightforward to consider for correlations with parameters derived from physical
932 volcanology.
933 - Multi-disciplinary correlations lead to improved understanding of explosion dynamics,
934 and only a complete set of measurements can enable a complete and well-constrained
935 understanding of the system (e.g., Gurioli et al. 2013; 2014; Leduc et al 2015).
936 - A wealth of textural and geophysical data exist for Strombolian events, and some data
937 for larger events. They have been used to define the characteristic geophysical and
938 textural signatures that allow distinguishing each event type (e.g. Patrick et al. 2007;
939 Leduc et al 2015). Focus on such relatively low energy events is appropriate, because
940 they are frequent and approachable (Harris and Ripepe 2007).
941 - There is an unfortunate, but understandable, lack of multi-disciplinary data for larger
942 (Vulcanian-to-Plinian) events; because they are rare. With multi-disciplinary
943 approaches becoming more routine, this situation is improving.
944 Thermal and SO_2 sensor arrays are becoming increasingly common components of permanent
945 monitoring arrays at many persistently active sites (Harris 2013). However, such technology

will probably never be installed on every potentially active volcano, all of which give seismic and pressure signals detectable by distant stations. From a practical point of view, it is more realistic to push forward with operational correlations between seismic-infrasonic metrics and deposit and particle textural deliverables to understand the ongoing progression of global volcanic events. In doing so, we must remember that many geophysical signals tend to be time-averages (e.g., tremor amplitude). We need to consider, however, geophysical measurements that describe single, discrete explosions if we are to reasonably compare the data with textural variations between many individual emission events, or emission phases, that characterize the total eruption total energy is one prime example (e.g., Marchetti et al 2009).

We are at an exciting point in our ability to track and understand explosive volcanic emissions through true cross-disciplinary integration of deposit, geochemical, textural and geophysical data. Studies are increasingly bringing together multiple approaches in the field (e.g., Rosi et al. 2006), in the laboratory (Clarke et al. 2009), at large-scale experiments (Sonder et al. 2013) and during field deployments (Harris et al. 2013b). As a community, we appear to be converging on the correct, multi-disciplinary approach. We are at the beginning of a new age, one which links particle texture to seismology (Miwa et al. 2009; Miwa and Toramaru 2013; Gurioli et al. 2014; Leduc et al. 2015) and infrasound (Colò et al. 2010, Landi et al. 2011); as well as petrology to geophysics (Saunders et al. 2012; Martí et al. 2013). Continuation of this trajectory can be aided by further support for pan-disciplinary workshops, meetings and working groups, the objectives of which are to totally understand the system and to constrain measurements with the least uncertainty.

Questions, needs and recommendations

Tables 2–4 summarize the main results from the previous discussions. Table 2 is the summary of major conclusions to date from cross-disciplinary approaches. Table 3 suggests improvements to methods to facilitate cross-disciplinary approaches. Finally, Table 4 groups outstanding questions that might be addressed if the recommended methods are used.

The list of key issues and questions defined allows us to distil the following community-wide points and initiatives as priorities:

1. We need to define, and adhere to, standard sampling, data collection, experimental and methodological procedures to allow full integration of the four disciplines;

2. In doing this, we need to understand each other's needs, and then follow each other's well-recognized sampling etiquette in order to work together as a truly integrated team;
3. We should aim to collate all data and measurements that can be provided by each discipline at some central host site and evaluate whether we need more from each field;
4. Quantification and statement of the precision of the measurements must always be made, and a set of standards must be produced to allow data quality control has to be followed;
5. The community needs to explore and discuss the best means to improve the quality of the measurements and the amount of data available;
6. Guidelines should be agreed on regarding essential key parameters that need to be extracted, versus those that are less important. Common standards need to be established that allow these key parameters to be shared by all groups;
7. Central to this is creation of an open access data bank to support essential geophysical, deposit, textural and geochemical data integration and sharing. This means creation of a repository of data grouped by eruptive style and/or geographic location into which members can make deposits and withdrawals;
8. All of this should ideally be integrated into a GIS platform to allow for easy cross-correlation and comparison of different types of parameters.

DynVolc: an integrated database

Inspired by this effort, a database – DynVolc (Dynamics of Volcanoes) – is now operative at http://wwwobs.univ-bpclermont.fr/SO/televolc/dynvolc/index.php. This database is part of an observation system within the services provided by Observatoire de Physique du Globe de Clermont-Ferrand (OPGC). It is an attempt to provide an integrated and accessible library for all multi-disciplinary data sets for explosive eruptive events. This database is an integrated collection of data from physical and geophysical observations of dynamic volcanic processes.

DynVolc database spans the full range of explosive and effusive activity. Its intent is to provide a library of standards for eruptive styles, for each of which the data base provides:

- field data (i.e., results of field mapping, outcrop and sample descriptions)
- key deposit features (thickness, areal dispersion, sedimentary structure, grain size)
- clast characterization (componentry, morphology, density, porosity, permeability)

- clast texture (connectivity, vesicle and crystal size and size distributions)
- chemical analyses of samples (bulk and glass chemistry
- associated geophysical measurements (e.g., fragmentation depth, ejection and ascent velocity, fragment and gas mass, seismic and acoustic energies)

Integration of these data allows improved, better constrained, insights into the dynamics driving each eruptive style. It also allows improved definition of the rheological and degassing conditions associated with each activity style. At the same time it provides a library of key physical parameters that need to be assumed by geophysical data reduction methods, as well as during model-based enquiry.

Central to this initiative will be the transformation of this database into a communal databank, involving a web-based GIS platform to allow huge amounts of cross-correlationand comparison between parameters relating to different processes and cross-correlation of different datasets obtained for the same eruption. It is intended as an open database into which anyone can input, and withdraw, citable cross-disciplinary information for scientific analysis. At the same time, through this library, we can provide cross-community time series, baseline and monitoring data for the full range volcanic activity.

Acknowledgements

L Gurioli thanks the MeMoVolc, European Science Foundation grant (ref. n. 4253). G Valentine D Swanson and the editor, J White are thanked for their constructive reviews. This research was financed by the French Government Laboratory of Excellence initiative no ANR-10-LABX-0006, the Région Auvergne, and the European Regional Development Fund. This is Laboratory of Excellence ClerVolc contribution number XXX

References

Adams NK, Houghton BF, Hildreth W (2006a) Abrupt transitions during sustained explosive eruptions: examples from the 1912 eruption of Novarupta, Alaska. Bull Volcanol 69:189–206

Adams NK, Houghton BF, Fagents S, Hildreth W (2006b) The transition from explosive to effusive eruptive regime: The example of the 1912 Novarupta eruption, Alaska. GSA Bulletin 118 (5/6):620–634. doi: 10.1130/B25768.1

1045 Alfano F, Bonadonna C, Volentik ACM, Connor CB, Watt SFL, Pyle DM, Connor LJ (2011)
1046 Tephra stratigraphy and eruptive volume of the May, 2008, Chaiten eruption, Chile. Bull
1047 Volcanol 73 (5):613–630
1048
1049 Alfano F, Bonadonna C, Gurioli L (2012) Insights on rhyolitic eruption dynamic from textural
1050 analysis: the example of the May Chaitén eruption (Chile). Bull Volcanol 74(9):2095-2108. doi
1051 10.1007/s00445-012-0648-3
1052
1053 Aloisi M, D'Agostino M, Dean KG, Mostaccio A and Neri G (2002). Satellite analysis and
1054 PUFF simulation of the eruptive cloud generated by the Mount Etna paroxysm of 22 July
1055 1998. J Geophys Res 107(B12): 2373. doi: 10.1029/2001JB000630
1056
1057 Anderson AT (1991) Hourglass inclusions: theory and application to the Bishop Rhyolitic
1058 Tuff. Am Min 76:530-547
1059
1060 Andronico D, Corsaro RA, Cristaldi A, Polacci M (2008) Characterizing high energy
1061 explosive eruptions at Stromboli volcano using multidisciplinary data: an example from the 9
1062 January 2005 explosion. J Volcanol Geotherm Res 176:541–550.
1063 doi:10.1016/j.jvolgeores.2008.05.011
1064
1065 Andronico D, Scollo S, Cristaldi A, Ferrari F (2009a), Monitoring ash emission episodes at
1066 Mt. Etna: The 16 November 2006 case study. J Volcanol Geotherm Res 180 (2–4):123–134.
1067 doi:10.1016/j. jvolgeores.2008.10.019
1068
1069 Andronico D, Cristaldi A, Del Carlo P, Taddeucci J (2009b) Shifting styles of basaltic
1070 explosive activity during the 2002-03 eruption of Mt Etna, Italy. J Volcanol Geotherm Res
1071 180(2-4):110-122. doi:10.1016/j.jvolgeores.2008.07.026
1072
1073 Andronico D, Lo Castro MD, Sciotto M, Spina L (2013a) The 2010 ash emissions at the
1074 summit craters of Mt Etna: Relationship with seismo-acoustic signals. J Geophys Res 118:51–
1075 70. doi:10.1029/2012JB009895
1076

1077 Andronico D, Taddeucci J, Cristaldi A, Miraglia L; Scarlato P, Gaeta M (2013b) The 15
1078 March 2007 paroxysm of Stromboli: video-image analysis, and textural and compositional
1079 features of the erupted deposit. Bull Volcanol 75:733. doi 10.1007/s00445-013-0733-2
1080
1081 Aoyama H and Oshima H (2008) Tilt change recorded by broadband seismometer prior to
1082 small phreatic explosion of Meakan-dake volcano, Hokkaido, Japan. Geophys Res Lett 35.
1083 doi:10.1029/2007GL032988
1084
1085 Armienti P (2008) Decryption of igneous textures: crystal size distribution tools. Rev Mineral
1086 Geochem 69:623-649
1087
1088 Armienti P, Tarquini S (2002) Power law olivine crystal size distributions in lithospheric
1089 mantle xenoliths. Lithos 65:273–285
1090
1091 Armienti P, Pareschi M, Innocenti F, Pompilio M (1994) Effects of magma storage and ascent
1092 on the kinetics of crystal growth. The case of the 1991-92 Mt.Etna eruption. Contrib Mineral
1093 Petr 115:402–414
1094
1095 Arzilli F, Voltolini M, Mancini L, Cicconi MR, Giuli G, Carroll MR (2013) Spherulites in
1096 trachytic melts. Mineral Mag 77(5):622
1097
1098 Asimow PD, Ghiorso MS (1998) Algorithmic modifications extending MELTS to calculate
1099 subsolidus phase relations. Am Mineral 83:1127–1131
1100
1101 Bai L, Baker DR, Rivers M (2008) Experimental study of bubble growth in Stromboli basalt
1102 melts at 1 atmosphere. Earth Planet Sci Lett 267:533–547. doi:10.1016/j.epsl.2007.11.063
1103
1104 Bai L, Baker DR, Hill RJ (2010) Permeability of vesicular Stromboli basaltic glass: Lattice
1105 Boltzmann simulations and laboratory measurements. J Geophys Res 115:B07201.
1106 doi:10.1029/2009JB007047
1107
1108 Bai L, Baker DR, Polacci M, Hill RJ (2011) In-situ degassing study on crystal-bearing
1109 Stromboli basaltic magmas: implications for Stromboli explosions. Geophys Res Lett
1110 38:L17309. doi.org/10.1029/2011GL048540

1111

1112 Baker DR, Polacci M, LaRue A (2011) A study on the reproducibility of counting vesicles in
1113 volcanic rocks. Geosphere 7:70-78
1114

1115 Baker DR, Mancini L, Polacci M, Higgins MD, GAR. Gualda, R.J. Hill, M.L. Rivers (2012)
1116 An introduction to the application of X-ray microtomography to the three-dimensional study
1117 of igneous rocks. Lithos 148:262-276
1118

1119 Balcone-Boissard H, Villemant B, Boudon G (2010) Behavior of halogens during the
1120 degassing of felsic magma. Geochem Geophys Geosyst 11(9):477–485.
1121 doi:10.10029/2010GC003028
1122

1123 Balcone-Boissard H, Boudon G, Villemant B (2011) Textural and geochemical constraints on
1124 eruptive style of the 79AD eruption at Vesuvius. Bull Volcanol. doi 10.1007/s00445-010-
1125 0409-0

1126 Balcone-Boissard H, Boudon G, Ucciani G, Villemant B, Cioni R, Civetta L, Orsi G (2012).
1127 Magma degassing and eruption dynamics of the Avellino Pumice Plinian eruption of Somma-
1128 Vesuvius (Italy). Comparison with the Pompeii eruption. Earth Planet Sci Lett 331-332:257-
1129 268. doi: 10.1016/j.epsl.2012.03.011
1130

1131 Barsotti S, Neri A, Scire JS (2008). The VOL-CALPUFF model for atmospheric ash
1132 dispersal: 1. Approach and physical formulation. J Geophys Res 113:B03208.
1133 doi:10.1029/2006JB004623
1134

1135 Barker SJ, Rotella MD, Wilson CJN, Wright IC, Wysoczanski RJ (2012) Contrasting
1136 pyroclast density spectra from subaerial and submarine silicic eruptions in the Kermadec arc:
1137 implications for eruption processes and dredge sampling Bull Volcanol 74:1425–1443.
1138 doi:10.1007/s00445-012-0604-2
1139

1140 Barnie T, Bombrun M, Burton MR, Harris A and Sawyer G (2014) Quantification of gas and
1141 solid emissions during Strombolian explosions using simultaneous sulphur dioxide and
1142 infrared camera observations. J Volcanol Geotherm Res
1143 http://dx.doi.org/10.1016/j.jvolgeores.2014.10.003

Bear J (1972) Dynamics of fluids in porous media. Dover, New York

Belien IB, Cashman KV, Rempel AW (2010), Gas accumulation in particle-rich suspensions and implications for bubble populations in crystal-rich magma. Earth Planet Sci Lett 297(1-2):133-140. doi:10.1016/j.epsl.2010.06.014

Berlo K, Turner S (2010) ^{210}Pb-^{226}Ra disequilibria in volcanic rocks. Earth Planet Sci Lett (Frontiers) 296:155-164

Berlo K, Blundy J, Turner S, Cashman K, Hawkesworth C, Black S (2004) Geochemical precursors to volcanic activity at Mount St. Helens, USA. Science 306:1167-1169

Bernard B (2013) Home-made ashmeter: a low-cost, high-efficiency solution to improve tephra field-data collection for contemporary explosive eruptions. J Appl Volcanol 2:1

Bernard ML, Zamora M, Geraud Y, Boudon G (2007) Transport properties of pyroclastic rocks from Montagne Pele´e volcano (Martinique, Lesser Antilles). J Geophys Res 112:B05205.doi.org/10.1029/2006JB004385

Bindeman IN (2003) Crystal sizes in evolving silicic magma chambers. Geology 31:367-370

Bjornsson H, Magnusson S, Arason P and Petersen GN (2013) Velocities in the plume of the 2010 Eyjafjallajökull eruption. J Geophys Res Atmos 118:698–711 doi:10.1002/jgrd.50876

Blower JD (2001a) Factors controlling permeability-porosity relationships in magma. Bull Volcanol 63:497–504

Blower JD (2001b) A three-dimensional network model of permeability in vesicular material. Comp Geosci 27:115–119

Blower JD, Keating JP, Mader HM, Phillips JC (2001) Inferring volcanic degassing processes from bubble size distributions. Geophys Res Lett 28(2):347–350

1178 Blower JD, Keating JP, Mader HM, Phillips JC (2002) The evolution of bubble size
1179 distributions in volcanic eruptions. J Volcanol Geother Res 120:1–23.
1180 http://dx.doi.org/10.1016/S0377-0273(02)00404-3
1181
1182 Blundy J, Cashman KV (2008) Petrologic reconstruction of magmatic system variables and
1183 processes. Rev Mineral Geochem 69:179–239.
1184
1185 Blundy J, Cashman K, Humphreys M (2006) Magma heating by decompression-driven
1186 crystallization beneath andesite volcanoes. Nature 443:76-80
1187
1188 Bombrun M, Barra V, Harris A (2014) Algorithm for particle detection and parameterization
1189 in high-frame-rate thermal video. J Appl Remote Sens 8(1):083549.
1190 doi:10.1117/1.JRS.8.083549
1191
1192 Bonadonna C, Costa A (2012) Estimating the volume of tephra deposits: A new simple
1193 strategy. Geology 40 (5):415–418. doi:10.1130/G32769.1
1194
1195 Bonadonna C, Ernst GGJ, Sparks RSJ (1998) Thickness variations and volume estimates of
1196 tephra fall deposits: the importance of particle Reynolds number. J Volcanol Geotherm Res
1197 81:173–187
1198
1199 Bonadonna C, Genco R, Gouhier M, Pistolesi M, Cioni R, Alfano F, Hoskuldsson A, Ripepe
1200 M (2011) Tephra sedimentation during the 2010 Eyjafjallajökull eruption (Iceland) from
1201 deposit, radar, and satellite observations. J Geophys Res 116(B12202).
1202 doi:10.1029/2011JB008462
1203
1204 Boorman S, Boudreau AE, Kruger FJ (2004) The lower zone–critical zone transition of the
1205 Bushveld complex: a quantitative textural study. J Petrol 45:1209–1235
1206
1207 Bouma AH (1969) Methods for the study of sedimentary structures. Jhon Wiley and Sons,
1208 New York, p 458
1209

1210 Bouvet de Maisonneuve C, Bachmann O, Burgisser A (2009) Characterization of juvenile
1211 pyroclasts from the Kos Plateau Tuff (Aegean Arc): insights into the eruptive dynamics of a
1212 large rhyolitic eruption. Bull Volcanol 71:643-658
1213
1214 Braun T, Ripepe M (1993) Interaction of seismic and air waves as recorded at Stromboli
1215 volcano. Geophys Res Lett 20(1):65–68
1216
1217 Brodsky E, Kanamori H, Sturtevant B (1999) A seismically constrained mass discharge rate
1218 for the initiation of the May 18, 1980 Mount St. Helens eruption. J Geophys Res 104:29,387–
1219 29,400
1220
1221 Bryon DN, Atherton MP, Hunter RH (1995) The interpretation of granitic textures from serial
1222 thin sectioning, image analysis and three-dimensional reconstruction. Miner Magaz 59:203-
1223 211
1224
1225 Burbié T, Zinszner B (1985) Hydraulic and acoustic properties as a function of porosity in
1226 Fontainebleau sandstone. J Geophys Res 90:11524–11532
1227
1228 Burgisser A, Gardner JE (2005) Experimental constraints on degassing and permeability in
1229 volcanic conduit flow. Bull Volcanol 67:42–56
1230
1231 Burgisser A, Poussineau S, Arbaret L, Druitt TH, Giachetti T, Bourdier JL (2010) Pre-
1232 explosive conduit conditions of the 1997 Vulcanian explosions at Soufrière Hills Volcano
1233 (Montserrat): I. pressure and vesicularity distributions. J Volcanol Geotherm Res 194 (1–
1234 3):27–41. doi:10.1016/j.jvolgeores.2010.01.008
1235
1236 Burton MR, Mader HM, Polacci M (2007) The role of gas percolation in quiescent degassing
1237 of persistently active volcanoes. Earth Planet Sci Lett 264:46–60.
1238 doi:10.1016/j.epsl.2007.08.028
1239
1240 Bustillos J, Mothes P (2010) Ash falls at Tungurahua volcano: implementation of systematic
1241 ash collection for quantifying accumulated volumes, Cities On Volcanoes abstract volume,
1242 Tenerife. Canary Island, Spain, May 31 – June 42010, 2.7-O-07
1243

1244 Büttner R, Dellino P, Zimanowski B (1999) Identifying magma–water interaction from the
1245 surface features of ash particles. Nature 401:688– 690
1246
1247 Büttner R, Dellino P, La Volpe L, Lorenz V, Zimanowsky B (2002) Thermohydraulic
1248 explosions in phreatomagmatic eruptions as evidenced by the comparison between pyroclasts
1249 and products from Molten Fuel Interaction experiments. J Geophys Res 107 (B11):2277.
1250 doi:10.1029/2001JB000511.
1251
1252 Cadoux A, Scaillet B, Druitt TH, Deloule E (2014). Magma storage conditions of large
1253 Plinian eruptions of SantoriniVolcano (Greece). J Petrology 55(6):1129-1171.
1254 doi:10.1093/petrology/egu021
1255
1256 Caltabiano T, Roman R and Budetta G (1994) SO2 flux measurements at Mount Etna (Sicily).
1257 J Geophys Res 99:12 809 – 12 819
1258
1259 Capaccioni B, Sarocchi D (1996) Computer-assisted image analysis on clast shape fabric from
1260 the Orvieto-Bagnoregio ignimbrite (Vulsini District, central Italy): implications on the
1261 emplacement mechanisms. J Volcanol Geotherm Res 70(1–2):75-90. doi: 10.1016/0377-
1262 0273(95)00049-6
1263
1264 Caracciolo C, Prodia F, Uijlenhoetc R (2006) Comparison between Pludix and impact/optical
1265 disdrometers during rainfall measurement campaigns. Atmos Res 82(1-2):137–163
1266
1267 Carey RJ, Houghton BF, Thordarson T (2009) Abrupt shifts between wet and dry phases of
1268 the 1875 eruption of Askja Volcano: microscopic evidence for macroscopic dynamics. J
1269 Volcanol Geotherm Res 184:256–270
1270
1271 Carey RJ, Manga M, Degruyter W, Swanson D, Houghton B, Orr T, Patrick M (2012)
1272 Externally triggered renewed bubble nucleation in basaltic magma: The 12 October 2008
1273 eruption at Halema‘uma‘u Overlook vent, Kīlauea, Hawai‘i, USA. J Geophys Res
1274 117:B11202. doi:10.1029/2012JB009496
1275
1276 Carey RJ, Manga M, Degruyter W, Gonnermann H, Swanson D, Houghton B, Orr T, Patrick
1277 M (2013) Convection in a volcanic conduit recorded by bubbles. Geology 41(4):395–398

Carey S, Sparks RSJ (1986) Quantitative models of the fallout and dispersal of tephra from volcanic eruption columns. Bull Volcanol 48:109–125. doi:10.1007/BF01046546

Carey S, Maria A, Sigurdsson H (2000) Use of fractal analysis for discrimination of particles from primary and reworked jökulhlaup deposits in SE Iceland. J Volcanol Geotherm Res 104:65–80

Carn SA, Krueger AJ, Bluth GJS, Schaefer SJ, Krotkov NA, Watson IM, Datta S (2003) Volcanic eruption detection by the Total Ozone Mapping Spectrometer (TOMS) instruments: a 22-year record of sulfur dioxide and ash emissions. In: Volcanic Degassing (eds. C Oppenheimer, DM Pyle and J Barclay), Geological Society, London, Special Publications, 213, pp.177-202.

Carn SA, Strow LL, de Souza-Machado S, Edmonds Y, Hannon S (2005) Quantifying tropospheric volcanic emissions with AIRS: the 2002 eruption of Mt. Etna (Italy). Geophys Res Lett 32(2):L02301. doi:10.1029/2004GL021034

Cas RAF, Wright JV (1987) Volcanic successions: modern and ancient. Allen & Unwin, London, 528p

Cashman KV (1988) Crystallization of Mount St. Helens 1980–1986 dacite: A quantitative textural approach. Bull Volcanol 50(3):194-209. doi:10.1007/BF01079682

Cashman KV (1992) Groundmass crystallization of Mount St. Helens dacite, 1980-1986: A tool for interpreting shallow magmatic processes. Contrib Mineral Petrol 109:431-449

Cashman KV (1993). Relationship between plagioclase crystallization and cooling rate in basaltic melts. Contrib Mineral Petr 113:126-142

Cashman KV, Mangan MT (1994) Physical aspects of magmatic degassing II. Constraints on vesiculation processes from textural studies of eruptive products. In: M. Carroll (Editor), Volatiles in Magmas. Mineral Sot Am Washington, DC, pp. 447-478

1312 Cashman KV, Marsh BD (1988) Crystal size distribution (CSD) in rocks and the kinetics and
1313 dynamics of crystallization II. Makaopuhi lava lake. Contrib Mineral Petrol 99:292–305
1314
1315 Cashman KV, McConnell S (2005) Transitions from explosive to effusive activity – the
1316 summer 1980 eruptions of Mount St. Helens. Bull Volcanol 68:57-75
1317
1318 Cashman KV, Mangan MT, Newman S (1994) Surface degassing and modifications to vesicle
1319 size distributions in Kilauea basalt. J Volcanol Geotherm Res 61:45-68
1320
1321 Castro JM, Cashman KV, Manga M (2003) A technique for measuring 3D crystal-size
1322 distributions of prismatic microlites in obsidian. Am Mineral 88:1230-1240
1323
1324 Castro JM, Burgisser A, Shipper CI, Mancini S (2012) Mechanisms of bubble coalescence in
1325 silicic magmas. Bull Volcanol 74:2339-2352
1326
1327 Chakraborty S (2008) Diffusion in solid silicates: A tool to track timescales of processes
1328 comes of age. Annu Rev Earth Planet Sci 36 (1):153-190
1329
1330 Chen Y, Provost A, Schiano P, Cluzel N (2011) The rate of water loss from olivine-hosted
1331 melt inclusions. Contrib Mineral Petrol 162:625-636
1332
1333 Chen Y, Provost A, Schiano P, Cluzel N (2013) Magma ascent rate and initial water
1334 concentration inferred from diffusive water loss from olivine-hosted melt inclusions. Contrib
1335 Mineral Petrol 165:525-541
1336
1337 Cheng HC, Lemlich R (1983) Errors in the measurement of bubble-size distribution in foam.
1338 Ind. Eng Chem Fundam 22:105–109
1339
1340 Chouet B, Hamisevicz N, McGetchin TR (1974) Photoballistics of volcanic jet activity at
1341 Stromboli, Italy. J Geophys Res 79:4961–4976
1342

1343 Cichy SB, Botcharnikov RE, Holtz F, Behrens H (2011) Vesiculation and microlite
1344 crystallization induced by decompression: a case study of the 1991-1995 Mt Unzen eruption
1345 (Japan). J Petrol 52:1469-1492
1346
1347 Cigolini C, Laiolo M, Bertolino S (2008) Probing Stromboli volcano from the mantle to
1348 paroxysmal eruptions. In: Annen C, Zellmer GF (eds) Dynamics of crustal magma transfer,
1349 storage and differentiation. Geological Society, London, special publication, vol 304.
1350 Geological Society, London, pp 33–70
1351
1352 Cimarelli C, Di Traglia F, Taddeucci J (2010) Basaltic scoria textures from a zoned conduit as
1353 precursors to violent Strombolian activity. Geology 38(5): 439-442
1354
1355 Cioni R, D'Oriano C, Bertagnini A (2008) Fingerprinting ash deposits of small scale eruptions
1356 by their physical and textural features. J Volcanol Geotherm Res 177:277–287
1357
1358 Cioni R, Bertagnini A, Andronico D, Cole PD, Mundula F (2011) The 512 AD eruption of
1359 Vesuvius: complex dynamics of a small scale subplinian event. Bull Volcanol 73 (7):789-810.
1360 doi:10.1007/s00445-011-0454-3
1361
1362 Clarke AB, Stephens S, Teasdale R, Sparks RSJ, Diller K (2007) Petrologic constraints on the
1363 decompression history of magma prior to Vulcanian explosions at the Soufrière Hills volcano,
1364 Montserrat. J Volcanol Geotherm Res 161:261-274
1365
1366 Clarke AB, Phillips JC, Chojnicki KN (2009) An investigation of Vulcanian eruption
1367 dynamics using laboratory analogue experiments and scaling analysis. In: Studies in
1368 Volcanology: The Legacy of George Walker, Thordason T, Self S, Larsen G, Rowland SK,
1369 Höskuldsson Á (eds) IAVCEI Special Publications in Volcanology 2: 155-166.
1370
1371 Cluzel N, Laporte D, Provost A (2008) Kinetics of heterogeneous bubble nucleation in
1372 rhyolitic melts: implications for the number density of bubbles in volcanic conduits and for
1373 pumice textures. Contrib Mineral Petrol 156:745-763
1374

1375 Colò L, Ripepe M, Baker DR, Polacci M (2010), Magma vesiculation and infrasonic activity
1376 at Stromboli open conduit volcano. Earth Planet Sc Lett 292 (3–4)
1377
1378 Colucci S, Palladino DM, Mulukutla GK, Proussevitch AA (2013) 3-D reconstruction of ash
1379 vesicularity: Insight into the origin of ash-rich explosive eruptions. J Volcanol Geotherm Res
1380 255:98-107
1381
1382 Costa F, Cohmen R, Chakraborty S (2008) Time scales of magmatic processes from modeling
1383 the zoning patterns of crystals. In Putirka KD, Tepley FJ (Eds) Minerals, inclusions and
1384 volcanic processes. Rev Mineral Geochem 69:545-594
1385
1386 Costantini L, Houghton BF, Bonadonna C (2010) Constraints on eruption dynamics of
1387 basaltic explosive activity derived from chemical and microtextural study: the example of the
1388 Fontana Lapilli Plinian eruption, Nicaragua. J Volcanol Geother Res 189 (3–4):207–224.
1389 doi:10.1016/j.jvolgeores.2009.11.008
1390
1391 Couch S, Sparks RSJ, Carroll MR (2003) The kinetics of degassing-induced crystallization at
1392 Soufrière Hills Volcano, Montserrat. J Petrol 44(8):1477–1502
1393
1394 De Campos CP, Dingwell DB, Perugini D, et al. (2008) Heterogeneities in magma chambers:
1395 Insights from the behavior of major and minor elements during mixing experiments with
1396 natural alkaline melts. Chem Geol 256:131–145. doi: 10.1016/j.chemgeo.2008.06.034
1397
1398 De Keyser TL (1999) Digital scanning of thin sections and peels. J Sedim Res 69:962–964
1399
1400 Degruyter W, Bachmann O, Burgisser A (2010a) Controls on magma permeability in the
1401 volcanic conduit during the climactic phase of the Kos Plateau Tuff eruption (Aegean Arc).
1402 Bull Volcanol 72:63–74. doi: 10.1007/s00445-009-0302-x
1403
1404 Degruyter W, Burgisser A, Bachmann O, Malaspina O (2010b) Synchrotron X-ray
1405 microtomography and lattice Boltzmann simulations of gas flow through volcanic pumices.
1406 Geosphere 6:470–481
1407

1408 Degruyter W, Bachmann O, Burgisser A, Manga M (2012) The effects of outgassing on the
1409 transition between effusive and explosive silicic eruptions. Earth Planet Sc Lett 349-350:161-
1410 170
1411
1412 Dehn J, Dean K, Engle K (2000) Thermal monitoring of North Pacific volcanoes from space.
1413 Geology 28(8):755-758
1414
1415 Dehn J, Dean KG, Engle K, Izbekov P (2002) Thermal precursors in satellite images of the
1416 1999 eruption of Shishaldin volcano. Bull Volcanol 64:525-545
1417
1418 Delle Donne D, Ripepe M (2012) High-frame rate thermal imagery of Strombolian
1419 explosions: Implications for explosive and infrasonic source dynamics. J Geophys Res
1420 117(B12). doi: 10.1029/2011JB008987
1421
1422 Dellino P, La Volpe L (1996a) Image processing analysis in reconstructing fragmentation and
1423 transportation mechanisms of pyroclastic deposits. the case of Monte Pilato-Rocche Rosse
1424 eruptions, Lipari (Aeolian Islands, Italy). J Volcanol Geotherm Res 71:13–29
1425
1426 Dellino P, La Volpe L (1996b) Cluster analysis on ash particles morphology features to
1427 discriminate fragmentation dynamics in explosive eruptions. Acta Vulcanologica 1:31–39
1428
1429 Dellino P, Liotino G (2002) The fractal and multifractal dimension of volcanic ash particles
1430 contour: a test study on the utility and volcanological relevance J Volcanol Geotherm Res 113
1431 (1–2):1-18. doi:10.1016/S0377-0273(01)00247-5
1432
1433 Dellino P, Isaia R, La Volpe L, Orsi G (2001) Statistical analysis of textural data from
1434 complex pyroclastic sequences: implications for fragmentation processes of the Agnano-
1435 Monte Spina Tephra (4.1 ka), Phlegraean Fields, southern Italy. Bull Volcanol 63:443–461
1436
1437 Dellino P, Mele D, Bonasia R, Braia G, La Volpe L, Sulpizio R (2005) The analysis of the
1438 influence of pumice shape on its terminal velocity. J Geophys Res 32:L21306.
1439 doi:10.1029/2005GL023954
1440

1441 Dellino P, Mele D, Sulpizio R, La Volpe L, Braia G (2012) A method for the calculation of
1442 the impact parameters of dilute pyroclastic density currents based on deposit particle
1443 characteristics. J Geophys Res 113 (B7). doi 10.1029/2007JB005365
1444
1445 Denniss AM, Harris AJL, Rothery DA, Francis PW, Carlton RW (1998) Satellite observations
1446 of the April 1993 eruption of Lascar volcano. Int J Remote Sensing 19(5):801-821
1447
1448 Dixon JE (1997) Degassing of alkali basalts. Am Min 82:368-378
1449
1450 Dohmen R, Becker H-W, Chakraborty S (2007) Fe–Mg diffusion in olivine I: experimental
1451 determination between 700 and 1,200°C as a function of composition, crystal orientation and
1452 oxygen fugacity. Phys Chem 34:389–407. doi: 10.1007/s00269-007-0157-7
1453
1454 D'Oriano C, Poggianti E, Bertagnini A, Cioni R, Landi P, Polacci M, Rosi M (2005) Changes
1455 in eruptive styles during the A.D. 1538 Monte Nuovo eruption (Phleagrean Fields, Italy): the
1456 role of syneruptive crystallization. Bull Volcanol 67:601–621
1457
1458 D'Oriano C, Cioni R, Bertagnini A, Andronico D, Cole PD (2011a) Dynamics of ash-
1459 dominated eruptions at Vesuvius: the post-512 AD AS1a event. Bull Volcanol 73 (6):699-
1460 715. doi:10.1007/s00445-010-0432-1
1461
1462 D'Oriano C, Bertagnini A, Pompilio M (2011b) Ash erupted during normal activity at
1463 Stromboli (Aeolian Islands, Italy) raises questions on how the feeding system works. Bull
1464 Volcanol 73:471-477
1465
1466 D'Oriano C, Pompilio M, Bertagnini A, Cioni R, Pichavant M (2012) Effects of experimental
1467 reheating of natural basaltic ash at different temperatures and redox conditions. Contrib
1468 Mineral Petrol. doi: 10.1007/s00410-012-0839-0
1469
1470 Dubosclard G, Cordesses R, Allard P, Hervier C, Coltelli C, Kornprobst J (1999) First testing
1471 of a volcano Doppler radar (Voldorad) at Mount Etna, Italy. Geophys Rese Lett 26(22):3389–
1472 3392
1473

1474 Eichelberger JC, Carrigan CR, Westrich HR, Price RH (1986) Non-explosive silicic
1475 volcanism. Nature 323:598–602
1476
1477 Engwell SL, Sparks RSJ, Aspinall WP (2013) Quantifying uncertainties in the measurement
1478 of tephra fall thickness. J Applied Volcanol 2:5. doi:10.1186/2191-5040-2-5.
1479
1480 Ersoy O, Chinga G, Aydar E, Gourgaud A, Cubuku HE, Ulusoy I (2006) Texture
1481 discimination of volcanic ashes from different fragmenation mechanisms: A case study,
1482 Mount Nemrut stratovolcano, eastern Turkey. Comput Geosci 32:936-946
1483
1484 Eychenne J, Le Pennec JL, Troncoso L, Gouhier M, Nedelec JM (2012) Causes and
1485 consequences of bimodal grainsize distribution of tephra fall deposited during the August
1486 2006 Tungurahua eruption (Ecuador). Bull Volcanol 74:187–205. doi: 10.1007/s00445-011-
1487 0517-5
1488
1489 Eychenne J, Le Pennec JL, Ramón P, Yepes H (2013) Dynamics of explosive paroxysms at
1490 open-vent andesitic systems: High-resolution mass distribution analyses of the 2006
1491 Tungurahua fall deposit (Ecuador). Earth Planet Sci Lett 361:343-355. doi: 10.10-
1492 16/j.epsl.2012.11.002
1493
1494 Eychenne J, Houghton BF, Swanson DA, Carey RJ, Swavely L (2015) Dynamics of an open
1495 basaltic magma system: The 2008 activity of the Halemaʻumaʻu Overlook vent, Kīlauea
1496 Caldera. Earth Planet Sci Lett 409:49-60
1497
1498 Fagents SA, Gregg TKP, Lopes RMC (2013) Modeling Volcanic Processes. The Physics and
1499 Mathematics of Volcanism. Cambridge University Press
1500
1501 Faure F, Trolliard G, Nicollet C, Montel J-M (2003) A developmental model of olivine
1502 morphology as a function of the cooling rate and the degree of undercooling. Contrib Mineral
1503 Petrol 145 (2):251–263. doi: 10.1007/s00410-003-0449-y
1504
1505 Faure F, Schiano P, Trolliard G, Nicollet C, Soulestin B (2007) Textural evolution of
1506 polyhedral olivine experiencing rapid cooling rates. Contrib Mineral Petrol 153:405-416
1507

1508 Ferguson DJ; Plank TA; Hauri EH; Houghton BF; Gonnermann HM; Swanson DA; Blaser
1509 AP (2013) Comparing eruptions of varying intensity at Kilauea via melt inclusion analysis.
1510 American Geophysical Union, Fall Meeting 2013, abstract #V33F-07
1511
1512 Fierstein J, Nathenson M (1992) Another look at the calculation of fallout tephra volumes.
1513 Bull Volcanol 54:156–167
1514
1515 Fierstein J, Houghton BF, Wilson CJN, Hildreth W (1997) Complexities of plinian fall
1516 deposition at vent: an example from the 1912 Novarupta eruption (Alaska). J Volcanol
1517 Geotherm Res 76:215–227
1518
1519 Fischer TP (2008) Fluxes of volatiles (H2O, CO2, N2, Cl, F) from arc volcanoes. Geochem J
1520 42:21–38. doi: 10.2343/geochemj.42.21
1521
1522 Fisher RV, Schmincke H-U (1984) Pyroclastic rocks. Springer, Berlin Heidelberg New York
1523
1524 Fiske RS, Rose TR, Swanson D, Champion D, McGeehin J (2009) Kulanaokuaiki Tephra (ca.
1525 A.D. 400–1000): Newly recognized evidence for highly explosive eruptions at Kīlauea
1526 Volcano, Hawai‘i." GSA Bull 121:712-728
1527
1528 Formenti Y, Druitt TH (2003) Vesicle connectivity in pyroclasts and implications for the
1529 fluidisation of fountain-collapse pyroclastic flows, Montserrat (West Indies). Earth Planet Sci
1530 Lett 214:561–574
1531
1532 Freundt A, Rosi M (1998) From Magma to Tephra. Elsevier, New York
1533
1534 Friese K-I, Cichy SB, Wolter F-E, Botcharnikov RE (2013). Analysis of tomographic mineral
1535 data using YaDiV – Overview and practical case study. Comput Geosci 56:92-103
1536
1537 Gaonac’h H, Lovejoy S, Stix J, Schertzer D (1996a) A scaling growth model for bubbles in
1538 basaltic flows. Earth Planet Sci Lett 139:395–409
1539
1540 Gaonac’h H, Stix J, Lovejoy S (1996b) Scaling effects on vesicles shape, size and
1541 heterogeneity of lavas from Mount Etna. J Volcanol Geotherm Res 74:131–153

1542
1543 Gaonac'h H, Lovejoy S, Schertzer D (2003) Percolating magmas and explosive volcanism.
1544 Geophys Res Lett 30. doi:10.1029/2002GL0116022
1545
1546 Gaonac'h H, Lovejoy S, Schertzer D (2005) Scaling vesicle distributions and volcanic
1547 eruptions. Bull Volcanol 67(4):350–357
1548
1549 Gardner JE (2007) Heterogeneous bubble nucleation in highly viscous silicate melts during
1550 instantaneous decompression from high pressure. Chem Geol 236:1-12

1551 Gaudin D, Moroni M, Taddeucci J, Scarlato P Shindler L. (2014a) Pyroclast Tracking
1552 Velocimetry: A particle tracking velocimetry-based tool for the study of Strombolian
1553 explosive eruptions. J Geophys Res Solid Earth 119:5369–5383. Doi:10.1002/2014JB011095

1554 Gaudin D, Taddeucci J, Scarlato P, Moroni M, Freda C, Gaeta M, Palladino DM (2014b)
1555 Pyroclast Tracking Velocimetry illuminates bomb ejection and explosion dynamics at
1556 Stromboli (Italy) and Yasur (Vanuatu) volcanoes. J Geophys Res Solid Earth 119:5384–5397.
1557 doi:10.1002/2014JB011096
1558
1559 Genareau K, Proussevitch AA, Durant AJ, Mulukutla GK, Sahagian DL (2012) Sizing up the
1560 bubbles that produce very fine ash during explosive volcanic eruptions. Geophys Res Lett
1561 39:(LI5306).
1562
1563 Genareau K, Mulukutla GK, Proussevitch AA, Durant AJ, Rose WI, Sahagian DL (2013) The
1564 size range of bubbles that produce ash during explosive volcanic eruptions. J Appl Volcanol
1565 2:4. doi:10.1186/2191-5040-2-4
1566
1567 Genco R, Ripepe M (2010) Inflation-deflation cycles revealed by tilt and seismic records at
1568 Stromboli volcano. Geophys Res Lett 37. doi: 10.1029/2010GL042925
1569
1570 Gerst A, Hort M, Aster RC, Johnson JB, Kyle PR (2013) The first second of volcanic
1571 eruptions from the Erebus volcano lava lake, Antarctica—Energies, pressures, seismology,
1572 and infrasound. J Geophys Res 118:3318–3340. doi:10.1002/jgrb.50234
1573

1574 Ghiorso MS, Sack RO (1995) Chemical mass transfer in magmatic processes. IV. A revised
1575 and internally consistent thermodynamic model for the interpolation and extrapolation of
1576 liquid-solid equilibria in magmatic systems at elevated temperatures and pressures. Contrib
1577 Mineral Petrol 119:197–212
1578
1579 Giachetti T, Gonnermann HM (2013).Water in pumices: rehydration or incomplete degassing?
1580 Earth Planet Sci Lett 369-370:317-332
1581
1582 Giachetti T, Druitt TH, Burgisser A, Arbaret L, Galven C (2010) Bubble nucleation and
1583 growth during the 1997 Vulcanian explosions of Soufrière Hills Volcano, Montserrat. J
1584 Volcanol Geotherm Res 193 (3–4):215–231. doi:10.1016/j.jvolgeores.2010.04.001
1585
1586 Giachetti T, Burgisser A, Arbaret L, Druitt TH, Kelfoun K (2011) Quantitative textural
1587 analysis of Vulcanian pyroclasts (Montserrat) using multi-scale X-ray computed
1588 microtomography: comparison with results from 2D image analysis. Bull Volcanol 73
1589 (9):1295-1309. doi:10.1007/s00445-011-0472-1
1590
1591 Goldstein P, Chouet B (1994) Array measurements and modeling of sources of shallow
1592 volcanic tremor at Kilauea Volcano, Hawaii. J Geophys Res 99(B2):2637–2652
1593
1594 Gonnermann HM, Houghton BF (2012) Magma degassing and fragmentation during the
1595 Plinian eruption of Novarupta, Alaska, 1912. Geochem Geophys Geosyst13:Q10009. doi: 10
1596 .1029 /2012GC004273
1597
1598 Gonnermann HM, Manga M (2013) Dynamics of magma ascent in the volcanic conduit. In
1599 Modelling volcanic processes: the physics and mathematics of volcanism, ed. By S. Fagents,
1600 T.K.P. Gregg, R.M.C. Lopes. Cambridge University Press, New York, pp. 55-84
1601
1602 Goodchild JS, Fueten F (1998) Edge detection in petrographic images using the rotating
1603 polarizer stage. Comput Geosci 24:745–751
1604
1605 Gouhier M, Donnadieu F (2008) Mass estimations of ejecta from Strombolian explosions by
1606 inversion of Doppler radar measurements. J Geophys Res 113:B10202.
1607 doi:10.1029/2007JB005383

Gouhier M, Donnadieu F (2011) Systematic retrieval of ejecta velocities and gas fluxes at Etna volcano using L-Band Doppler radar. Bull Volcanol 73(9):1139-1145. doi:10.1007/s00445-011-0500-1

Gualda GAR (2006) Crystal size distributions derived from 3D datasets: sample size versus uncertainties. J Petrol 47(6):1245-1254

Gualda GAR, Rivers M (2006) Quantitative 3D petrography using X- ray tomography: application to Bishop Tuff pumice clasts. J Volcanol Geotherm Res 154(1–2):48–62

Gualda GAR, Baker DR, Polacci M (2010a) Introduction: Advances in 3D imaging and analysis of Geomaterials, Geosphere, special issue "Advances in 3D Imaging and Analysis of Geomaterials" 6-5:468-469. doi:10.1130/GES00639.1

Gualda GAR, Pamukcu AS, Claiborne LL, Rivers ML (2010b) Quantitative 3D petrography using X-ray tomography 3: documenting accessory phases with differential absorption tomography. Geosphere 6(6):782–792

Gurioli L, Houghton B, Cashman K, Cioni R (2005) Complex changes in eruption dynamics and the transition between Plinian and phreatomagmatic activity during the 79AD eruption of Vesuvius. Bull Volcanol 67:144-159 doi: 10.1007/s00445-004-0368-4

Gurioli L, Harris AJL, Houghton BF, Polacci M, Ripepe M (2008) Textural and geophysical characterization of explosive basaltic activity at Villarrica volcano. J Geophys Res 113:B08206. doi:10.1029/2007JB005328

Gurioli L, Harris AJL, Colò L, Bernard J, Favalli M, Ripepe M, Andronico D (2013) Classification, landing distribution and associated flight parameters for a bomb field emplaced during a single major explosion at Stromboli, Italy. Geology 41 (5):559–562. doi 10.1130/G33967.1

1640 Gurioli L, Colò L, Bollasina AJ, Harris AJL, Whittington A, Ripepe M (2014) Dynamics of
1641 strombolian explosions: inferences from inferences from field and laboratory studies of
1642 erupted bombs from Stromboli volcano. J Geophys Res 119. doi:10.1002/2013JB010355
1643
1644 Hamada M, Laporte D, Cluzel N, Koga KT (2010) Simulating bubble number density of
1645 rhyolitic pumices from Plinian eruptions: constraints from fast decompression experiments.
1646 Bull Volcanol 72:735-746
1647
1648 Hammer JE (2008). Experimental studies of the kinetics and energetics of magma
1649 crystallization. Rev Mineral Geochem 69:9-59
1650
1651 Hammer JE, Rutherford MJ (2002) An experimental study of the kinetics of decompression-
1652 induced crystallization in silicic melt. J Geophys Res 107(B1). doi:10.1029/2001JB000281
1653
1654 Hammer JE, Cashman KV, Hoblitt RP, Newman S (1999) Degassing and microlite
1655 crystallization during pre-climactic events of the 1991 eruption of Mt. Pinatubo, Philippines.
1656 Bull Volcanol 60:355–380
1657
1658 Hammer JE, Sharp TG, Wessel P (2010) Heterogeneous nucleation and epitaxial crystal
1659 growth of magmatic minerals. Geology 38: 367-370.
1660
1661 Harris A (2013) Thermal Remote Sensing of Active Volcanoes: A User's Manual, Cambridge
1662 University Press: 728 p.
1663
1664 Harris AJL, Ripepe M (2007) Synergy of multiple geophysical approaches to unravel
1665 explosive eruption conduit and source dynamics – A case study from Stromboli. Chemie der
1666 Erde 67: 1-35.
1667
1668 Harris AJL, Ripepe M, Hort M (2004) Foreward. J Volcanol Geotherm Res 137(1-3):vii– viii.
1669 doi:10.1016/S0377-0273(04)00276-8
1670
1671 Harris AJL, Ripepe M, Hughes EE (2012) Detailed analysis of particle launch velocities, size
1672 distributions and gas densities during normal explosions at Stromboli. J Volcanol Geotherm
1673 Res 231-232:109-131

Harris AJL, Delle Donne D, Dehn J, Ripepe M, Worden K (2013a) Volcanic plume and bomb field masses from thermal infrared camera imagery. Earth Planet Sci Lett 365:77-85. doi: 10.1016/j.epsl.2013.01.004

Harris AJL, Battaglia J, Donnadieu F, Gurioli L, Kelfoun K, Labazuy P, Sawyer G, Valade S, Bombun M, Barra V, Delle Donne D, Lacanna G (2013b) Full bandwidth remote sensing for total parameterization of volcanic plumes. EOS 94 (37):321-322

Heiken G and Pitts DE (1975) Identification of eruption clouds with the landsat satellites. Bull Volcanol 39(2):255-265

Heiken G, Wohletz KH (1985) Volcanic ash, University of California Press, Berkeley, Ca, USA

Heilbronner R (2000) Automatic grain boundary detection and grain size analysis using polarization micrographs or orientation images. J Struct Geol 22:969–981

Herd R, Pinkerton H (1997) Bubble coalescence in basaltic lava: its impact on the evolution of bubble populations. J Volcanol Geotherm Res 75:137–157

Higgins MD (2000) Measurement of crystal size distributions Am Mineral 85:1105–1116

Higgins MD (2002a) A crystal size-distribution study of the Kiglapait layered mafic intrusion, Labrador, Canada: Evidence for textural coarsening. Contrib Mineral Petr 144:314-330

Higgins MD (2002b) Closure in crystal size distributions (CSD), verification of CSD calculations, and the significance of CSD fans. Am Mineral 87:171-175

Higgins MD (2006) Quantitative textural measurements in igneous and metamorphic petrology. Cambridge University Press, Cambridge

Higgins MD (2011) Textural coarsening in igneous rocks. Int Geol Rev 53:354–376

1708 Hoblitt RP, Harmon RS (1993) Bimodal density distribution of cryptodome dacite from the
1709 1980 Mount St. Helens, Washington. Bull Volcanol 55:421– 437
1710
1711 Holasek RE, Self S (1995) GOES weather satellite observations and measurements of the
1712 May 18, 1980, Mount St. Helens eruption. J Geophys Res 100(B5):8469-8487
1713
1714 Holasek RE, Self S, Woods AW (1996) Satellite observations and interpretation of the 1991
1715 Mount Pinatubo eruption plumes. J Geophys Res 101(B12):27635-27655
1716
1717 Holland ASP, Watson M, Phillips JC, Caricchi L, Dalton MP (2011) Degassing processes
1718 during lava dome growth: Insights from Santiaguito lava dome, Guatemala. J Volcanol
1719 Geotherm Res 202(1–2):153-166
1720
1721 Hort M, Seyfried R, Vöge M (2003) Radar Doppler velocimity of volcanic eruptions:
1722 Theoretical considerations and quantitative documentation of changes in eruptive behaviour at
1723 Stromboli volcano, Italy. Geophys J Int 154:515-532
1724
1725 Hort M, Seyfried R (1998) Volcanic eruption velocities measured with a micro radar.
1726 Geophys Res Lett 25:113–116
1727
1728 Horton K, Williams-Jones G, Garbeil H, Elias T, Sutton AJ, Mouginis-Mark P, Porter JN,
1729 Clegg S (2005) Real-time measurement of volcanic SO2 emissions: validation of a new UV
1730 correlation spectrometer (FLYSPEC). Bull Volcanol: doi 10.1007/s00445-005-0014-9
1731
1732 Houghton BF, Wilson CJN (1989) A vesicularity index for pyroclastic deposits. Bull
1733 Volcanol 51:451–462. doi:10.1007/BF01078811
1734
1735 Houghton BF, Carey RJ, Cashman KV, Wilson CJN, Hobden BJ, Hammer JE (2010) Diverse
1736 patterns of ascent, degassing, and eruption of rhyolite magma during the 1.8 ka Taupo
1737 eruption, New Zealand: Evidence from clast vesicularity, J Volcanol Geotherm Res 195:31–
1738 47
1739

1740 Houghton BF, Swanson DA, Rausch J, Carey RJ, Fagents SA, Orr TR (2013) Pushing the
1741 Volcanic Explosivity Index to its limit and beyond: Constraints from exceptionally weak
1742 explosive eruptions at Kılauea in 2008. Geology 41(6):627–630
1743
1744 Humphreys MCS, Menand T, Blundy JD, Klimm K (2008a) Magma ascent rates in explosive
1745 eruptions: constraints from H2O diffusion in melt inclusions. Earth Planet Sci Lett 270:25-40
1746
1747 Humphreys MC, Blundy JD, Sparks RSJ (2008b) Shallow-level decompression crystallization
1748 and deep magma supply at Shiveluch volcano. Contrib Mineral Petrol 155:45-61
1749
1750 Hurwitz S, Navon O (1994) Bubble nucleation in rhyolitic melts: experiments at high
1751 pressure, temperature, and water content. Earth Planet Sci Lett 122:267-280
1752
1753 Iguchi M, Yakiwara H, Tameguri T, Hendrasto M, Hirabayashi J (2008) Mechanism of
1754 explosive eruption revealed by geophysical observations at the Sakurajima, Suwanosejima
1755 and Semeru volcanoes. J Volcanol Geotherm Res 178(1):1-9
1756
1757 Innocenti S, Andreastuti S, Furman T, del Marmol M-A, Voight B (2013) The pre-eruption
1758 conditions for explosive eruptions at Merapi volcano as revealed by crystal texture and
1759 mineralogy. J Volcanol Geother Res doi.org/10.1016/j.jvolgeores.2012.12.028
1760
1761 Ishibashi H, Sato H (2007) Viscosity measurements of subliquidus magmas: alkali olivine
1762 basalt from the Higashi-Matsuura district, Southwest Japan. J Volcanol Geotherm Res
1763 160:223–238
1764
1765 Jerram DA, Cheadle MJ, Philpotts AR (2003) Quantifying the building blocks of igneous
1766 rocks: are clustered crystal frameworks the foundation? J Petrol 44:2033–2051
1767
1768 Jouniaux L, Bernard ML, Zamora M, Pozzi JP (2000) Streaming potential in volcanic rocks
1769 from Mount Pelée. J Geophys Res 105:8391–8401
1770
1771 Kahl M, Chakraborty S, Costa F, Pompilio M (2011) Dynamic plumbing system beneath
1772 volcanoes revealed by kinetic modeling, and the connection to monitoring data: An example
1773 from Mt. Etna. Earth Planet Sc Lett 308:11–22. doi: 10.1016/j.epsl.2011.05.008

Kaneshima S, Kawakatsu H, Matsubayashi H, Sudo Y, Tsutsui T, Ohminato T, Ito H, Uhira K, Yamasato H, Oikawa J, Takeo M, Iidaka T (1996) Mechanism of phreatic eruptions at Aso Volcano inferred from near-field broadband seismic observations. Science 273(5275):643-645

Kennedy B, Spieler O, Scheu B, Kueppers U, Taddeucci J, Dingwell DB (2005) Conduit implosion during Vulcanian eruptions. Geology 33:581-584. doi: 10.1130/G21488.1

Kent AJR (2008) Melt inclusions in basaltic and related volcanic rocks. Rev Mineral Geochem 69: 273-331

Kent AJR, Blundy J, Cashman K, Cooper KM, Donnelly C. et al. (2007) Vapor transfer prior to the October 2004 eruption of Mount St. Helens, Washington. Geology 35: 231–234

Ketcham RA (2005) Computational methods for quantitative analysis of three-dimensional features in geological specimens. Geosphere 1:32-41

Ketcham RA, Carlson WD (2001) Acquisition, optimization and interpretation of X-ray computed tomographic imagery: applications to the geosciences. Comput Geosci 27:381–400

Klawonn M, Houghton BF, Swanson DA,. Fagents SA, Wessel P, Wolfe CJ (2014) Constraining explosive volcanism: subjective choices during estimates of eruption magnitude. Bull Volcanol 76:793. doi: 10.1007/s00445-013-0793-3

Klug C, Cashman KV (1994) Vesiculation of May 18, 1980, Mount St. Helens magma. Geology 22:468–472

Klug C, Cashman KV (1996) Permeability development in vesiculating magmas: implications for fragmentation. Bull Volcanol 58:87–100

Klug C, Cashman KV, Bacon CR (2002) Structure and physical characteristics of pumice from the climatic eruption of Mount Mazama (Crater Lake), Oregon. Bull Volcanol 64:486–501

1808 Koyaguchi T, Tokuno M (1993) Origin of the giant eruption cloud of Pinatubo, June 15,
1809 1991. J Volcanol Geotherm Res 55:85-96
1810
1811 Krueger AJ, Walter LS, Doiron SD (1990) TOMS measurement of sulfur dioxide emitted
1812 during the 1985 Nevado del Ruiz eruptions. J Volcanol Geotherm Res 41:7-15
1813
1814 Kueppers U, Scheu B, Spieler O, Dingwell DB (2005) Field-based density measurements as
1815 tool to identify pre-eruption dome structure: set-up and first results from Unzen volcano,
1816 Japan. J Volcanol Geotherm Res 141:65–75
1817
1818 Kueppers U, Scheu B, Spieler O, Dingwell DB (2006) Fragmentation efficiency of explosive
1819 volcanic eruptions: A study of experimentally generated pyroclasts. J Volcanol Geotherm Res
1820 153(1–2):125-135
1821
1822 Kyser TK, O'Neil JR (1984) Hydrogen isotope systematic of submarine basalts. Geochim
1823 Cosmochim Acta 48:2123–2133
1824
1825 Lak M, Néraudeau D, Nel A, Cloetens P, Perrichot V, Tafforeau P (2008) Phase contrast X-
1826 ray synchrotron imaging: opening access to fossil inclusions in opaque amber. Microsc
1827 Microanal 14(3):251–259
1828
1829 Landi P, Marchetti E, La Felice S, Ripepe M, Rosi M (2011) Integrated petrochemical and
1830 geophysical data reveals thermal distribution of the feeding conduits at Stromboli volcano,
1831 Italy. Geophys Res Lett 38:L08305
1832
1833 Lanza R, Meloni A (2006) The Earth's magnetism: an introduction for geologists. 278 pp.
1834 Berlin, Heidelberg, New York: Springer-Verlag
1835
1836 Larsen JF (2008) Heterogeneous bubble nucleation and disequilibrium H2O exsolution in
1837 Vesuvius K-phonolite melts. J Volcanol Geotherm Res 275:278–288
1838
1839 Larsen JF, Gardner JE (2000) Experimental constraints on bubble interactions in rhyolite
1840 melts: implications for vesicle size distributions. Earth Planet Sci Lett 180:201–214
1841

LaRue A, Baker DR, Polacci M, Allard P, Sodini N (2013), Can vesicle size distributions assess eruption intensity during volcanic activity? J Geophys Res-Solid Earth 4:373–80. doi:10.5194/se-4-373-2013

Laumonier M, Arbaret L, Burgisser A, Champallier R (2011) Porosity redistribution enhanced by strain localization in crystal-rich magmas. Geology 39:715–718. http://dx.doi.org/10.1130/G31803.1

Launeau P, Cruden AR (1998) Magmatic fabric acquisition mechanisms in a syenite: results of a combined anisotropy of magnetic susceptibility and image analysis study. J Geophys Res 103:5067–5089

Launeau P, Bouchez JL, Benn K (1990) Shape preferred orientation of object populations: Automatic analysis of digitized images. Tectonophysics 180:201-211

Launeau P, Cruden AR, Bouchez JL (1994) Mineral recognition in digital images of rocks: a new approach using multichannel classification. Can Mineral 32:919–933

Lautze NC, Houghton BF (2005) Physical mingling of magma and complex eruption dynamics in the shallow conduit at Stromboli volcano, Italy. Geology 33:425–428.

Lautze NC, Houghton BF (2007) Linking variable explosion style and magma textures during 2002 at Stromboli volcano, Italy. Bull Volcanol 69:445–460

Lautze NC, Houghton BF (2008) Single explosions at Stromboli in 2002: use of clast microtextures to map physical diversity across a fragmentation zone. J Volcanol Geotherm Res 170:262–268

Lautze N, Taddeucci J, Andronico D, Cannata C, Tornetta L, Scarlato P, Houghton B, Lo Castro D (2012) SEM-based methods for the analysis of basaltic ash from weak explosive activity at Etna in 2006 and the 2007 eruptive crisis at Stromboli. Phys Chem Earth 45–46:113–127. doi:10.1016/j.pce.2011.02.001

1875 Lautze N, Taddeucci J, Andronico D, Houghton B, Niemeijer A, Scarlato P (2013) Insights
1876 into explosion dynamics and the production of ash at Stromboli from samples collected in real
1877 time, October 2009. Geol S Am S 498:125-139
1878
1879 Lavallée Y, Varley N, Alatorre-Ibargüengoitia MA, Hess KU, Mueller S, Richard D, Scheu
1880 B, Spieler O, Dingwell DB (2012) Magmatic architecture of dome-building eruptions at
1881 Volcán de Colima, Mexico. Bull Volcanol 74:249-260
1882
1883 Leduc L, Gurioli L, Harris AJL, Colò L, Rose-Koga E Dynamics of a gas-dominated
1884 strombolian explosion. Bull Volcanol 77:8. doi: 10.1007/s00445-014-0888-5.
1885
1886 Le Losq C, Neuville DR, Moretti R, Roux J (2012) Determination of water content in silicate
1887 glasses using Raman spectrometry: Implications for the study of explosive volcanism. Am
1888 Mineral 97:779-790
1889
1890 Le Pennec JL, Hermitte D, Isya D, Pezard P, Coulon C, Cochemé J-J, Mulyadi E, Ollagnier
1891 F,Revest C (2001). Electrical conductivityand pore-space topology of Merapi lavas:
1892 implication for the degassing of porphyritic andesite magmas. Geophys Res Lett
1893 28(22):4283–4286
1894
1895 Le Voyer M, Rose-Koga EF, Shimizu N, Grove TL, Schiano P (2010) Two contrasting H_2O-
1896 rich components in primary melt inclusions from Mount Shasta. J Petrol 5(7):1571–1595. doi:
1897 10.1093/petrology/egq030
1898
1899 Lesne P, Kohn SC, Blundy J, Witham F, Botcharnikov RE, Behrens H. (2011). Experimental
1900 simulation of closed-system degassing in the system basalt-H_2O-CO_2-S-Cl. J Petrol 52:1737-
1901 1762
1902
1903 Liu Y, Anderson AT, Wilson CJN (2007) Melt pockets in phenocrysts and decompression
1904 rates of silicic magmas before fragmentation. J Geophys Res 112. doi:10.1029/2006JB004500
1905
1906 Lovejoy S, Gaonac'h H, Schertzer D (2004) Bubble distributions, and dynamics: the
1907 expansion-coalescence equation. J Geophys Res 109:B11203. doi:10.1029/2003JB002823
1908

1909 Lumbreras F, Serrat J (1996) Segmentation of petrographical images of marbles. Comput
1910 Geosci 22:547–558
1911
1912 Magee C, O'Driscoll B, Chambers AD (2010) Crystallization and textural evolution of a
1913 closed-system magma chamber: insights from a crystal size distribution study of the Lilloise
1914 layered intrusion, east Greenland. Geol Mag 147:363–379
1915
1916 Manga M. (1998) Orientation distribution of microlites in obsidian. J Volcanol Geother Res
1917 86:107–115
1918
1919 Mangan M (1990) Crystal size distribution systematics and the determination of magma
1920 storage times: The 1959 eruption of Kilauea volcano, Hawaii. J Volcanol Geother Res
1921 44:295–302
1922
1923 Mangan MT, Cashman, KV (1996) The structure of basaltic scoria and reticulite and
1924 inferences for vesiculation, foam formation, and fragmentation in lava fountains. J Volcanol
1925 Geotherm Res 73:1-18
1926
1927 Mangan M, Sisson T (2000) Delayed, disequilibrium degassing in rhyolite magma:
1928 decompression experiments and implications for explosive volcanism. Earth Planet Sci Lett
1929 183:441–55
1930
1931 Mangan M, Sisson T (2005). Evolution of melt-vapor surface tension in silicic volcanic
1932 systems: Experiments with hydrous melts. J Geophys Res 110:B01202. doi:
1933 10.1029/2004JB003215
1934
1935 Mangan MT, Cashman KV, Newman S (1993) Vesiculation of basaltic magma during
1936 eruption. Geology 21:157–160
1937
1938 Marchetti E, Ripepe M, Harris AJL, Delle Donne D (2009) Tracing the differences between
1939 Vulcanian and Strombolian explosions using infrasonic and thermal radiation energy. Earth
1940 Planet Sci Lett 279:273–281
1941

1942 Marchetti E, Poggi P, Bonadonna C, Pistolesi M, Hoskuldsson A (2013) Towards real-time
1943 measurements of tephra fallout grain-size distribution. MeMoVolc Meeting, Geneve
1944 Switzerland, Jannuary 2014
1945
1946 Maria A, Carey S (2002) Using fractal analysis to quantitatively characterize the shapes of
1947 volcanic particles. J Geophys Res 107:(B11):2283. doi:10.1029/2001JB000822
1948
1949 Maria A, Carey S (2007) Quantitative discrimination of magma fragmentation and pyroclastic
1950 transport processes using the fractal spectrum technique. J Volcanol Geotherm Res 161:234–
1951 246
1952
1953 Marsh BD (1988) Crystal size distribution (CSD) in rocks and the kinetics and dynamics of
1954 crystallization: I. Theory. Contrib Mineral Petrol 99:277– 291
1955
1956 Marsh BD (1998) On the interpretation of crystal size distributions in magmatic systems. J
1957 Petrol 39:553–599
1958
1959 Marsh BD (2007) Crystallization of silicate magmas deciphered using crystal size
1960 distributions. J Am Ceramic Society 90:746-757
1961
1962 Marshall JR (1987) Clastic particles: Scanning electron microscopy and shape analysis of
1963 sedimentary and volcanic clasts, Van Nostrand Reinhold Company, New York, 346 p.
1964
1965 Marschallinger R (1998a) A method for three-dimensional reconstruction of macroscopic
1966 features in geological materials. Comput Geosc 24:875-883
1967
1968 Marschallinger R (1998b) Correction of geometric errors associated with the 3-D
1969 reconstruction of geological materials by precision serial lapping. Mineral Mag 62:783-792
1970
1971 Marschallinger R (1998c) 3-D reconstruction and volume modelling of the grain fabric of
1972 geological materials. Phys Chem Earth 23:267-271
1973

1974 Martel C (2012) Eruption Dynamics inferred from microlite crystallization experiments:
1975 application to Plinian and dome-forming eruptions of Mt. Pelée (Martinique, Lesser Antilles).
1976 J Petrol 53:699-725
1977
1978 Martel C, Radadi Ali A, Poussineau S, Gourgaud A, Pichavant M (2006) Basalt-inherited
1979 microlites in silicic magmas: evidence from Mt. Pelée (Martinique, F.W.I.). Geology 34:905–
1980 908
1981
1982 Marti J, Soriano C, Dingwell DB (1999) Tube pumices as strain markers of the ductile-brittle
1983 transition during magma fragmentation. Nature 402(6762):650–653
1984
1985 Martí J, Castro A, Rodríguez C, Costa F, Carrasquilla S, Pedreira R, Bolos X (2013)
1986 Correlation of magma evolution and geophysical monitoring during the 2011–2012 El Hierro
1987 (Canary Islands) submarine eruption. J Petrology 54(7):1349-1373.
1988 doi:10.1093/petrology/egt014.
1989
1990 Mattsson HB (2010) Textural variation in juvenile pyroclasts from an emergent, Surteyan-
1991 type, volcanic eruption: The Capelas tuff cone, São Miguel (Azores). J Volcanol Geoth Res
1992 189:81–91
1993
1994 McNutt SR (1986) Observations and analysis of B-type earthquakes, explosions, and volcanic
1995 tremor at Pavlof Volcano, Alaska. Bull Seis Soc Amer 76:153-175
1996
1997 Mele D, Dellino P, Sulpizio R, Braia G (2011) A systematic investigation on the
1998 aerodynamics of ash particles, J Volcanol Geotherm Res 203:1–11.
1999 doi:10.1016/j.jvolgeores.2011.04.004
2000
2001 Melnik O, Sparks RSJ (2002) Dynamics of magma ascent and lava extrusion at Soufrière
2002 Hills Volcano, Montserrat. In: Druitt, T., Kokelaar, B. (Eds.), The Eruption of Soufrière Hills
2003 Volcano, Montserrat, from 1995 to 1999. The Geological Society of London, pp. 153–171.
2004
2005 Métrich N, Bertagnini A, Landi P, Rosi M (2001), Crystallization driven by decompression
2006 and water loss at Stromboli volcano (Aeolian Islands, Italy). J Petrol 42:1471–1490.
2007 doi:10.1093/petrology/42.8.1471

Métrich N, Wallace PJ (2008) Volatile abundances in basaltic magmas and their degassing paths tracked by melt inclusions. In Putirka KD, Tepley FJ (Eds) Minerals, inclusions and volcanic processes Rev Mineral Geochem 69:363-402

Métrich N, Bertagnini A, Di Muro A (2010) Conditions of magma storage, degassing and ascent at Stromboli: new insights into the volcano plumbing system with inferences on the eruptive dynamics. J Petrol 51(3):603-626

Miwa T, Toramaru A (2013) Conduit process in vulcanian eruptions at Sakurajima volcano, Japan: Inference from comparison of volcanich ash with pressure wave and seismic data. Bull Volcanol 75:685

Miwa T, Toramaru A, Iguchi M (2009) Correlations of volcanic ash texture with explosion earthquakes from vulcanian eruptions at Sakurajima volcano, Japan. J Volcanol Geotherm Res 184(3–4):473–486

Miwa T, Geshi N, Shinohara H (2013) Temporal variation in volcanic ash texture during a vulcanian eruption at the Sakurajima volcano, Japan. J Volcanol Geotherm Res 260:80-89

Mock A, Jerram DA (2005) Crystal size distributions (CSD) in three dimensions: Insights from the 3D reconstruction of a highly porphyritic rhyolite: J Petrol 46:1525–1541. doi: 10.1093/petrology/egi024

Mock A, Jerram DA, Breitkreuz C (2003) Using quantitative textural analysis to understand the emplacement of shallow-level rhyolitic laccoliths a case study from the Halle volcanic complex, Germany. J Petrol 44:833-849

Moitra P, Gonnermann HM, Houghton BF, Giachetti T (2013) Relating vesicle shapes in pyroclasts to eruption styles. Bull Volcanol 75:691. doi 10.1007/s00445-013-0691-8

Morgan DJ, Jerram DA, Chertkoff DG, Davidson JP, Pearson DG, Kronz A, Nowell GM (2007) Combining CSD and isotopic microanalysis: magma supply and mixing processes at Stromboli volcano, Aeolian islands, Italy. Earth Planet Sci Lett 260(3–4):419–431

Mori T, Burton M (2006) The SO2 camera: a simple, fast and cheap method for groundbased imaging of SO2 in volcanic plumes. Geophys Res Lett 33(L24804): doi:10.1029/2006GL027916

Mori T, Burton M (2009) Quantification of the gas mass emitted during single explosions on Stromboli with the SO2 imaging camera. J Volcanol Geotherm Res 188:395–400. doi:10.1016/j.jvolgeores.2009.10.005

Mori J, Patia H, McKee C, Itikarai I, Lowenstein P, De Saint Ours P, Talai B (1989) Seismicity associated with eruptive activity at Langila volcano, Papua New Guinea. J Volcanol Geotherm Res 38(3–4):243-255

Mourtada-Bonnefoi CC, Laporte D (2002) Homogenous bubble nucleation in rhyolitic magmas: An experimental study on the effect of H_2O and CO_2. J Geophys Res 107:B4. doi: 10.1029/2001JB000290

Mourtada-Bonnefoi CC, Laporte D (2004) Kinetics of bubble nucleation in a rhyolitic melt: an experimental study of the effect of ascent rate. Earth Planet Sci Lett 218:521-537

Mueller S, Melnik O, Spieler O, Scheu B, Dingwell DB (2005) Permeability and degassing of dome lavas undergoing rapid decompression: An experimental determination Bull Volcanol 67(6):526–538. doi:10.1007/s00445-004-0392-4

Mueller S, Scheu B, Spieler O, Dingwell DB (2008) Permeability control on magma fragmentation. Geology 36(5):399–402. doi:10.1130/G24605A.1

Mueller S, Scheu B, Kueppers U, Spieker O, Richard D, Dingwell DB (2011) The porosity of pyroclasts as an indicator of volcanic explosivity. J Volcanol Geotherm Res 203:168-174

Muir DD, Blundy JD, Rust AC (2012) Multiphase petrography of volcanic rocks using element maps: a method applied to Mount St. Helens, 1980–2005 Bull Volcanol 74:1101–1120

2076 Murtagh RM, White JDL (2013) Pyroclast characteristics of a subaqueous to emergent
2077 Surtseyan eruption, Black Point volcano, California. J Volcanol Geotherm Res 267:75:91
2078
2079 Murtagh RM, White JDL, Sohn YK (2011) Pyroclast textures of the Ilchulbong 'wet' tuff
2080 cone, Jeju Island, South Korea. J Volcanol Geotherm Res 201:385-396.
2081
2082 Nakamura K (2006) Textures of plagioclase microlite and vesicles within volcanic products
2083 of the 1914–1915 eruptions of Sakurajima Volcano, Kyushu, Japan. J Mineral Petrol Sci
2084 101:178–198
2085
2086 Nakamura M, Otaki K, Takeuchi S (2008) Permeability and pore-connectivity variation of
2087 pumices from a single pyroclastic flow eruption: Implications for partial fragmentation. J
2088 Vocanol Geotherm Res 176:302–314
2089
2090 Németh K (2010) Volcanic glass textures, shape characteristics and compositions of
2091 phreatomagmatic rock units from the Western Hungarian monogenetic volcanic fields and
2092 their implications for magma fragmentation. Cent Eur J Geosci 2:399–419
2093
2094 Neuberg J, Luckett R, Ripepe M, Braun T (1994) Highlights from a seismic broadband array
2095 on Stromboli volcano. Geophys Res Lett 21:749–752
2096
2097 Newman S, Lowenstern JB (2002) VolatileCalc: a silicate melt-H2O-CO2 solution model
2098 written in Visual Basic for Excel: Computers and Geosciences 28(5):597-604
2099
2100 Newman S, Epstein S, Stolper E (1988) Water, carbon dioxide, and hydrogen isotopes in
2101 glasses from the CA. 1340 A.D. eruption of the Mono Craters, California: constraints on
2102 degassing phenomena and initial volatile content. J Volcanol Geotherm Res 35:75-96
2103
2104 Nguyen CT, Gonnermann HM, Chen Y, Huber C, Maiorano AA, Gouldstone A, Dufek J
2105 (2013) Film drainage and the lifetime of bubbles. Geochem Geophys Geosyst 14:3616–3631
2106
2107 Nishimura T, McNutt SR (2008) Volcanic tremor during eruptions: temporal characteristics,
2108 scaling and estimates of vent radius. J Volcanol Geotherm Res 178:10-18
2109

2110 Noguchi S, Toramaru A, Shimano T (2006) Crystallization of microlites and degassing during
2111 magma ascent: Constraints on the fluid mechanical behavior of magma during the Tenjo
2112 Eruption on Kozu Island, Japan. Bull Volcanol 68:432–449. doi 10.1007/s00445-005-0019-4
2113
2114 Noguchi S, Toramaru A, Nakada S (2008) Relation between microlite textures and discharge
2115 rate during the 1991–1995 eruptions at Unzen, Japan. J Volcanol Geotherm Res 175(1–
2116 2):141–155
2117
2118 O'Driscoll B, Donaldson CH, Troll VR, Jerram DA, Emeleus CH (2007) An origin for
2119 harrisitic and granular olivine in the rum layered suite, NW Scotland: a crystal size
2120 distribution study. J Petrol 48(2):253–270
2121
2122 Okumura S, Nakamura M, Tsuchiyama A (2006) Shear-induced bubble coalescence in
2123 rhyolitic melts with low vesicularity. Geophys Res Lett 33:L20316.
2124 doi:10.1029/2006GL027347
2125
2126 Okumura S, Nakamura M, Tsuchiyama A, Nakano T, Uesugi K (2008) Evolution of bubble
2127 microstructure in sheared rhyolite: Formation of a channel-like bubble network: J Geophys
2128 Res 113:B07208. doi: 10.1029/2007JB005362
2129
2130 Okumura S, Nakamura M, Uesugi K, Nakano T, Fujioka T (2013) Coupled effect of magma
2131 degassing and rheology on silicic volcanism. Earth Planet Sci Lett 362:163–170
2132
2133 Oppenheimer C, Scaillet B, Martin RS (2011) Sulfur degassing from volcanoes: source
2134 conditions, surveillance, plume chemistry and impacts, Rev Mineral Geochem 73:363-421.
2135 doi:10.2138/rmg.2011.73.13
2136
2137 Palladino DM, Taddeucci J (1998) The basal ash deposit of the Sovana Eruption (Vulsini
2138 Volcanoes, central Italy): the product of a dilute pyroclastic density current. J Volcanol
2139 Geotherm Res 87:233–254
2140
2141 Pamukcu AS, Gualda GAR (2010) Quantitative 3D petrography using X-ray tomography 2:
2142 combining information at various resolutions. Geosphere 6:775–781.
2143 doi.org/10.1130/GES00565.1

2144

2145 Pamukcu AS, Gualda GAR, Anderson AT (2012) Crystallization stages of the Bishop Tuff
2146 magma body recorded in crystal textures in pumice clasts. J Petrol 63:589–609
2147

2148 Pardo N et al (2014a) Perils in distinguishing phreatic from phreatomagmatic ash; insights
2149 into the eruption mechanisms of the 6 August 2012 Mt. Tongariro eruption, New Zealand. J
2150 Volcanol Geotherm Res http://dx.doi.org/10.1016/j.jvolgeores.2014.05.001
2151

2152 Pardo N, Cronin SJ, Wright HMN, Schipper IC, Smith I, Stewart B (2014b) Pyroclast textural
2153 variation as an indicator of eruption column steadiness in andesitic Plinian eruptions at Mt.
2154 Ruapehu. Bull Volcanol 76:822
2155

2156 Patrick MR (2007) Dynamics of Strombolian ash plumes from thermal video: motion,
2157 morphology, and air entrainment. J Geophys Res 112:B06202. doi:10.1029/2006JB004387.
2158

2159 Perugini D, Poli G, Properini N (2002) Morphometric analysis of magmatic enclaves: a tool
2160 for understanding magma vesiculation and ascent. Lithos 61:225–235
2161

2162 Perugini D, Valentini L, Poli G (2007) Insights into magma chamber processes from the
2163 analysis of size distribution of enclaves in lava flows: a case study from Vulcano Island
2164 (Southern Italy). J Volcanol Geotherm Res 166:193–203
2165

2166 Perugini D, Speziali A, Caricchi L, Kueppers U (2011) Application of fractal fragmentation
2167 theory to natural pyroclastic deposits: Insights into volcanic explosivity of the Valentano
2168 scoria cone (Italy). J Volcanol Geotherm Res 202(3-4):200-210
2169

2170 Pfeiffer T, Costa A, Macedonio G (2005) A model for the numerical simulation of tephra fall
2171 deposits. J Volcanol Geotherm Res 140:273–294
2172

2173 Pickering G, Bull JM Sanderson DJ (1995) Sampling power-law distributions:
2174 Tectonophysics. 248:1–20. doi:10.1016/0040-1951(95)00030-Q
2175

2176 Pichavant M, Martel C, Bourdier JL, Scaillet B (2002) Physical conditions, structure, and
2177 dynamics of a zoned magma chamber: Mount Pelée (Martinique, Lesser Antilles Arc). J
2178 Geophys Res 107. doi:10.1029/2001JB000315
2179
2180 Pichavant M, Costa F, Burgisser A, et al. (2007) Equilibration scales in silicic to intermediate
2181 magmas: implications for experimental studies. J Petrol 48:1955–1972. doi:
2182 10.1093/petrology/egm045
2183
2184 Pichavant M, Carlo I, Rotolo SG, et al. (2013) Generation of CO2-rich melts during basalt
2185 magma ascent and degassing. Contrib Mineral Petr. doi: 10.1007/s00410-013-0890-5
2186
2187 Piochi M, Mastrolorenzo G, Pappalardo L (2005) Magma ascent and eruptive processes from
2188 textural and compositional features of Monte Nuovo pyroclastic products, Campi Flegrei,
2189 Italy. Bull Volcanol 67:663–678
2190
2191 Piochi M, Polacci M, De Astis G, Zanetti A, Mangiacapra A, Vannucci R, Giordano D (2008)
2192 Texture and composition from pumices and scoriae of the Campi Flegrei caldera (Italy):
2193 Implications on the dynamics of explosive eruptions. Geochem Geophys Geosyst 9:Q03013.
2194 doi:10.1029/2007GC001746
2195
2196 Pioli L, Erlund E, Johnson E, Cashman K, Wallace P, Rosi M, Delgado Granados H (2008)
2197 Explosive dynamics of violent strombolian eruptions: the eruption of Parícutin volcano 1943–
2198 1952 (Mexico). Earth Planet Sci Lett 271:359–368
2199
2200 Pioli L, Pistolesi M, Rosi M (2014) Transient explosions at open-vent volcanoes: the case of
2201 Stromboli (Italy). Geology 42:863-866
2202
2203 Pistolesi M, Rosi M, Pioli L, Renzulli A, Bertagnini A, Andronico D (2008), The paroxysmal
2204 explosion and its deposits, in The Stromboli Volcano: An Integrated Study of the 2002–2003
2205 Eruption, Geophys. Monogr. Ser. vol. 182, edited by S. Calvari et al. pp. 317–329, AGU,
2206 Washington, D. C. doi:10.1029/182GM26
2207

2208 Pistolesi M, Delle Donne D, Pioli L, Rosi M, Ripepe M (2011) The 15 March 2007 explosive
2209 crisis at Stromboli volcano, Italy: assessing physical parameters through a multidisciplinary
2210 approach. J Geophys Res 116(B12). doi: 958 10.1029/2011JB008527
2211
2212 Platz T, Cronin SJ, Cashman KV, Stewart RB, Smith IEM (2007) Transition from effusive to
2213 explosive phases in andesite eruptions — A case-study from the AD1655 eruption of Mt.
2214 Taranaki, New Zealand. J Volcanol Geotherm Res 161:15-34
2215
2216 Polacci M, P Papale, M Rosi (2001) Textural heterogeneities in pumices from the climatic
2217 eruption of Mount Pinatubo, 15 June 1991, and implications for magma ascent dynamics. Bull
2218 Volcanol 63:83–97
2219
2220 Polacci M, Pioli L, Rosi M (2003) The Plinian phase of the Campanian Ignimbrite eruption
2221 (Phlegrean Fields, Italy): evidence from density measurements and textural characterization of
2222 pumice. Bull Volcanol 65:418–432
2223
2224 Polacci M, Corsaro R, Andronico D (2006a) Coupled textural and compositional
2225 characterization of basaltic scoria: Insights into the transition from Strombolian to fire
2226 fountain activity at Mount Etna, Italy. Geology 34(3):201–204. doi:10.1130/G223181.1
2227
2228 Polacci M, Baker DR, Mancini L, Tromba G, Zanini F (2006b) Three-dimensional
2229 investigation of volcanic textures by X-ray microtomography and implications for conduit
2230 processes. Geophys Res Lett 33(13):L13312. doi:10.1029/2006GL026241
2231
2232 Polacci M, Baker DR, Bai L, Mancini L (2008) Large vesicles record pathways of degassing
2233 at basaltic volcanoes. Bull Volcanol 70:1023–1029. doi:10.1007/s00445-007-0184-8
2234
2235 Polacci M, Baker DR, Mancini L, Favretto S, Hill RJ (2009a) Vesiculation in magmas from
2236 Stromboli and implications for normal Strombolian activity and paroxysmal explosions in
2237 basaltic systems. J Geophys Res 114:B01206. doi.org/10.1029/2008JB005672
2238
2239 Polacci M, Burton MR, La Spina A, Murè F, Favretto S, Zanini F (2009b) The role of syn-
2240 eruptive vesiculation on explosive basaltic activity at Mt. Etna, Italy. J Volcanol Geotherm
2241 Res 179:265–269

Polacci M, Mancini L, Baker DR (2010) The contribution of synchrotron X-ray computed microtomography to understanding volcanic processes. J Synchrotron Radiation 17:215–221

Polacci M, Baker DR, La Rue A, Mancini L (2012) Degassing behaviour of vesiculated basaltic magmas: an example from Ambrym volcano, Vanuatu Arc, and comparison to Stromboli, Aeolian Islands, Italy. J Volcanol Geotherm Res 233-234:55-64. doi: 10.1016/j.jvolgeores.2012.04.019

Polacci M, Bouvet de Maisonneuve C, Giordano D, Piochi M, Mancini L, Degruyter W, Bachmanng O (2014) Permeability measurements of Campi Flegrei pyroclastic products: An example from the Campanian Ignimbrite and Monte Nuovo eruptions. J Volcanol Geotherm Res 272:16-22

Prata AJ (1989) Infrared radiative transfer calculations for volcanic ash clouds. Geophys Res Lett 15(11):1293–1296

Prata AJ, Bernardo C (2009) Retrieval of volcanic ash particle size, mass and optical depth from a ground-based thermal infrared camera. J Volcanol Geotherm Res 186:91–107

Prejean SG, Brodsky EE (2011) Volcanic plume height measured by seismic waves based on a mechanical model. J Geophys Res Solid Earth 116(B1. doi:10.1029/2010JB007620

Prior DJ (1999) Problems in determining the orientations of crystal misorientation axes, for small angular misorientations, using electron backscatter diffraction in the SEM. J Microsc 195:217–225

Prior DJ, Boyle AP, Brenker F, Cheadle MC, Day A, Lopez G, Peruzzo L, Potts GJ, Reddy S, Spiess R, Timms NE, Trimby P, Wheeler J, Zetterström L (1999) The application of electron backscatter diffraction and orientation contrast imaging in the SEM to textural problems in rocks. Am Mineral 84:1741–1759

2274 Prodi F, Caracciolo D, Adderio LP, Gnuffi M, Lanzinger E (2011) Comparative investigation
2275 of Pludix disdrometer capability as Present Weather Sensor (PWS) during the Wasserkuppe
2276 campaign. Atmos Res 99(1):162–173
2277
2278 Proussevitch AA, Sahagian DL, Tsentalovich EP (2007a) Statistical analysis of bubble and
2279 crystal size distributions: formulations and procedures. J Volcanol Geotherm Res 164:95–111
2280
2281 Proussevitch AA, Sahagian DL, Carlson W (2007b) Statistical analysis of bubble and crystal
2282 size distributions: application to Colorado Plateau basalts. J Volcanol Geotherm Res 164:112–
2283 126
2284
2285 Proussevitch AA, Mulukutla GK, Sahagian DL (2011) A new 3D method of measuring bubble
2286 size distributions from vesicle fragments preserved on surfaces of volcanic ash particles.
2287 Geosphere 7:1–8
2288
2289 Pyle M (1989) The thickness, volume and grainsize of tephra fall deposits. Bull Volcanol
2290 51:1–15
2291
2292 Pyle DM, Mather TA (2009) Halogens in igneous processes and their fluxes to the atmosphere
2293 and oceans from volcanic activity: A review: Chem Geol 263(1-4):110–121. doi:
2294 10.1016/j.chemgeo.2008.11.013
2295
2296 Riley CM, Rose WI, Bluth GJS (2003) Quantitative shape measurements of distal volcanic
2297 ash. J Geophys Res 108:B10. doi: 10.1029/2001JB000818
2298
2299 Ripepe M, Braun T (1994) Air-wave phases in strombolian explosion-quake seismograms: a
2300 possible indicator for the magma level? Acta Vulcanol 5:201–206
2301
2302 Ripepe M, Marchetti E (2002) Array tracking of infrasonic sources at Stromboli volcano.
2303 Geophys Res Lett 29 (22):2076
2304
2305 Ripepe M, Ciliberto S, Della Schiava M (2001) Time constraints for modeling source
2306 dynamics of volcanic explosions at Stromboli. J Geophys Res 106(B5):8713–8727
2307

2308 Ripepe M, Harris AJL, Carniel R (2002). Thermal, seismic and infrasonic evidences of
2309 variable degassing rates at Stromboli volcano. J Volcanol Geotherm Res 118:285–297
2310
2311 Ripepe M, Poggi P, Braun T, Gordeev E (1996) Infrasonic waves and volcanic tremor at
2312 Stromboli. Geophys Res Lett 23:181–184
2313
2314 Ripepe M, Rossi M, Saccorotti G (1993) Image processing of explosive activity at Stromboli.
2315 J Volcanol Geotherm Res 54:335–351
2316
2317 Rix M, Valks P, Hao N, Loyola D, Schlager H, Huntrieser H, Flemming J, Koehler U,
2318 Schumann U, Inness A (2012) Volcanic SO2, BrO and plume height estimations using
2319 GOME-2 satellite measurements during the eruption of Eyjafjallajökull in May 2010. J
2320 Geophys Res 117:D00U19. doi:10.1029/2011JD016718
2321
2322 Robock A, Matson M (1982) Circumglobal transport of the El Chichon volcanic dust cloud.
2323 Science 221:195-197
2324
2325 Roggensack K, hervig RL, McKnight SB, Williams SN (1997) Explosive basaltic volcanism
2326 from Cerro Negro volcano: influence of volatiles on eruptive style. Science 277:1639-1642
2327
2328 Rose WI, Self S, Murrow PJ, Bonadonna C, Durant AJ, Ernst GGJ (2008) Nature and
2329 significance of small volume fall deposits at composite volcanoes: Insights from the October
2330 14, 1974 Fuego eruption, Guatemala. Bull Volcanol 70(9):1043–1067
2331
2332 Rose-Koga EF, Koga K, Schiano P, Le Voyer M (2012) Mantle source heterogeneity for South
2333 Tyrrhenian magmas revealed by Pb isotopes and halogen contents of olivine-hosted melt
2334 inclusions. Chem Geol 334:266-279
2335
2336 Rosseel JB, White JDL, Houghton BF (2006) Complex bombs of phreatomagmatic eruptions:
2337 role of agglomeration and welding in vents of the 1886 Rotomahana eruption, Tarawera, New
2338 Zealand. J Geophys Res 111:B12205. doi:10.1029/2005JB004073
2339

2340 Rosi M, Bertagnini A, Harris AJL, Pioli L, Pistolesi M, Ripepe M (2006) A case history of
2341 paroxysmal explosion at Stromboli: Timing and dynamics of the April 5, 2003 event. Earth
2342 Planet Sci Lett 243:594–606
2343
2344 Rotella MD, Wilson CJN, Barker SJ, Wright IC (2013) Novel origins of highly vesicular
2345 pumice in a distinctive non-explosive submarine eruptive style. Nature Geosci 6:129–132
2346
2347 Rotella MD, Wilson CJN, Barker SJ, Cashman KV, Houghton BF, Wright IC (2013) Bubble
2348 development in explosive silicic eruptions: insights from pyroclast vesicularity textures from
2349 Raoul volcano (Kermadec arc). Bull Volcanol 76:826
2350
2351 Rust AC, Cashman KV (2004) Permeability of vesicular silicic magma: inertial and hysteresis
2352 effects. Earth Planet Sci Lett 228:93–107, http://dx.doi.org/ 10.1016/j.epsl.2004.09.025
2353
2354 Rust AC, Cashman KV (2007) Multiple origins of pyroclastic obsidian and implications for
2355 changes in the dynamics of the 1300 BP eruption of Newberry Volcano, OR. Bull Volcanol
2356 69:825-845
2357
2358 Rust AC, Cashman KV (2011) Permeability controls on expansion and size distributions of
2359 pyroclasts. J Geophys Res 116:B11202
2360
2361 Rust AC, Manga M, Cashman KV (2003) Determining flow type, shear rate and shear stress
2362 in magmas from bubble shapes and orientations. J Volcanol Geotherm Res 122:111–132
2363
2364 Ruth D, Calder E (2014) Plate tephra: Preserved bubble walls from large slug bursts during
2365 violent Strombolian eruptions. Geology 42(1):11–14, doi:10.1130/G34859.1
2366
2367 Rutherford MJ, Hill PM (1993) Magma ascent rates from amphibole breakdown: an
2368 experimental study applied to the 1980–1986 Mount St. Helens eruptions. J Geophys Res
2369 98:19667–19685
2370
2371 Rutherford MJ, Devine JD (2003) Magmatic conditions and magma ascent as indicated by
2372 hornblende phase equilibria and reactions in the 1995-2002 Soufrière Hills magma. J Petrol
2373 44:1433-1454

Rutherford MJ, Sigurdsson H, Carey S, Davis A (1985) The May 18, 1980 eruption of Mount St. Helens, 1. Melt compositions and experimental phase equilibria. J Geophys Res 90:2929-2947

Saar MO, Manga M (1999) Permeability-porosity relationship in vesicular basalts. Geophys Res Lett 26(1):111–114

Sable JE, Houghton BF, Del Carlo P, Coltelli M (2006) Changing conditions of magma ascent and fragmentation during the Etna 122 BC basaltic Plinian eruption: evidence from clast microtextures. J Volcanol Geotherm Res 158:333–354

Sable JE, Houghton BF, Wilson CJN, Carey RJ (2009) Eruption mechanisms during the climax of the Tarawera 1886 basaltic Plinian eruption inferred from microtextural characteristics of the deposits, in Studies in Volcanology: The Legacy of George Walker, Spec. Publ. IAVCEI, vol. 2, pp. 129–154, Geol. Soc., London

Sahagian DL, Proussevitch AA (1998) 3D particle size distributions from 2D observations: stereology for natural applications. J Volcanol Geotherm Res 84:173–196

Sahetapy-Engel ST, Harris AJL. (2009) Thermal-image-derived dynamics of vertical ash plumes at Santiaguito volcano, Guatemala. Bull Volcanol 71:827-830. doi:10.1007/s00445-009-0284-8

Salisbury MJ, Bohrson WA, Clynne MA, Ramos FC, Hoskin P (2008) Multiple plagioclase crystal populations identified by crystal size distribution and in situ chemical data: implications for timescales of magma chamber processes associated with the 1915 eruption of Lassen Peak, CA. J Petrol 49:1755–1780

Saunders K, Blundy J, Dohmen R, Cashman (2012) Linking petrology and seismology at an active volcano. Science 336(6084):1023-1027. doi:10.1126/science.1220066

Scaillet B, Evans BW (1999) The 15 June 1991 eruption of Mount Pinatubo. I. Phase equilibria and pre-eruption *P*-*T*-fO_2-fH_2O conditions of the dacite magma. J Petrol 40(3):381-411

Schiavi F, Kobayashi K, Moriguti T, et al. (2010) Degassing, crystallization and eruption dynamics at Stromboli: trace element and lithium isotopic evidence from 2003 ashes. Contrib Mineral Petr 159:541–561

Schiavi F, Kobayashi K, Nakamura E, et al. (2012) Trace element and Pb–B–Li isotope systematics of olivine-hosted melt inclusions: insights into source metasomatism beneath Stromboli (southern Italy). Contrib Mineral Petrol 163:1011-1031

Schipper CI, White JDL, Houghton BF (2010a) Syn- and post-fragmentation textures in submarine pyroclasts from Loihi Seamount, Hawaii. J Volcanol Geotherm Res 191:93–106. doi:10.1016/j/jvolgeores.2010.01.002

Schipper CI, White JDL, Houghton BF, Shimizu N, Stewart RB (2010b) Explosive submarine eruptions driven by volatile-coupled degassing at Lo`ihi Seamount, Hawai`i. Earth Planet Sci Lett 295(3-4):497-510

Schipper CI, White JDL, Houghton BF, Shimizu N, Stewart RB (2010c) "Poseidic" explosive eruptions at Loihi Seamount, Hawaii. Geology 38(4):291-294

Schipper CI, White JDL, Houghton BF (2011) Textural, geochemical, and volatile evidence for a Strombolian-like eruption sequence at Lō`ihi Seamount, Hawai`i. J Volcanol Geotherm Res 207:16–32

Schipper CI, White JDL, Nichols ARL, Burgisser A, Hellebrand E, Murtagh RM (2012) Incipient melt segregation as preserved in subaqueous pyroclasts. Geology 40(4):355-358

Schipper CI, Castro JM, Tuffen H, James MR, How P (2013) Shallow vent architecture during hybrid explosive-effusive activity at Cordón Caulle (Chile, 2011-12): evidence from direct observations and pyroclast textures. J Volcanol Geotherm Res 262:25–37

Sciotto M, Cannata A, Di Grazia G, Gresta S, Privitera E, Spina L (2011) Seismoacoustic investigations of paroxysmal activity at Mt. Etna volcano: New insights into the 16 November 2006 eruption. J Geophys Res 116. doi: 10.1029/2010JB008138

Shea T, Larsen JF, Gurioli L, Hammer JE, Houghton BF, Cioni R (2009) Leucite crystals: surviving witnesses of magmatic processes preceding the 79 AD eruption at Vesuvius, Italy. Earth Planet Sci Lett 281:88–98

Shea T, Houghton BF, Gurioli L, Cashman KV, Hammer JE, Hobden B (2010a) Textural studies of vesicles in volcanic rocks: an integrated methodology. J Volcanol Geotherm Res 190:271–289

Shea T, Gurioli L, Larsen JF, Houghton BF, Hammer JE, Cashman KV (2010b) Linking experimental and natural vesicle textures in Vesuvius 79 AD white pumice. J Volcanol Geotherm Res 192:69–84

Shea T, Gurioli L, Houghton BF, Cashman KV, Cioni R (2011) Column collapse and generation of pyroclastic density currents during the A.D. 79 eruption of Vesuvius: the role of pyroclast density. Geology 39:695–698

Shea T, Gurioli L, Houghton BF (2012) Transitions between fall phases and pyroclastic density currents during the AD 79 eruption at Vesuvius: building a transient conduit model from the textural and volatile record. Bull Volcanol 74:2363–2381. doi 10.1007/s00445-012-0668-z

Shea T, Hellebrand E, Gurioli L, Hugh T (2014) Conduit- to localized-scale degassing during Plinian eruptions: Insights from major element and volatile (Cl and H_2O) analysis within Vesuvius AD79 pumice. J Petrol. doi:10.1093/petrology/egt069

Sheridan MF, Marshall JR (1983) Interpretation of pyroclast surface features using SEM images. J Volcanol Geotherm Res 16:153–159

Sheridan MF, Marshall JR (1987) Comparative charts for quantitative analysis of grain-textural elements on pyroclasts, in Clastic Particles: Scanning Electron Microscopy And

Shape Analysis Of Sedimentary And Volcanic Particles, edited by J. R. Marshall, Van Nostrand Reinhold Company, New York

Shimano T, Nakada S (2006) Vesiculation path of ascending magma in the 1983 and the 2000 eruptions of Miyakejima volcano, Japan. Bull Volcanol 68:549–566. doi: 10.1007/s00445-005-0029-2

Shimano T, Nishimura T, Chiga N, Shibasaki Y, Iguchi M, Miki D and Yokoo A (2013) Development of an automatic volcanic ash sampling apparatus for active volcanoes. Bull Volcanol 75:73. doi: 10.1007/s00445-013-0773-7

Shin H, Lindquist WB, Sahagian DL, Song S-R (2005) Analysis of the vesicular structure of basalts. Comput Geosci 31(4):473–487. doi:10.1016/j.cageo.2004.10.013

Simakin AG, Bindeman IN (2008). Evolution of crystal sizes in the series of dissolution and precipitation events in open magma systems. J Volcanol Geotherm Res 17:997-1010

Simkin T, Howard KA (1970) Caldera Collapse in the Galápagos Islands, 1968 The largest known collapse since 1912 followed a flank eruption and explosive volcanism within the caldera. Science 169(3944):429-437

Sonder I, Graettinger A, Valentine G (2013) Large-scale blast experiments examine subsurface explosions. EOS Trans AGU 94(39):337–338. doi:10.1002/2013EO390002

Song SR, Jones KW, Lindquist WB, Dowd BA, Sahagian DL (2001) Synchrotron X-ray computed microtomography: studies on vesiculated basaltic rocks. Bull Volcanol 63(4):252–263. doi:10.1007/s004450100141

Sottili G, Taddeucci J, Palladino DM, Gaeta M, Scarlato P, Ventura G (2009) Subsurface dynamics and eruptive styles of maars in the Colli Albani Volcanic District, Central Italy. J Volcanol Geotherm Res 180:189-202

Sottili G, Taddeucci J, Palladino DM (2010) Constraints on magma–wall rock thermal interaction during explosive eruptions from textural analysis of cored bombs. J Volcanol Geotherm Res 192:27-34

Sparks RSJ (1978) The dynamics of bubble formation and growth in magmas. J Volcanol Geotherm Res 3:1–37. doi:10.1016/0377-0273(78)90002-1

Sparks RSJ, Brazier S (1982) New evidence for degassing processes during explosive eruptions. Nature 295:218–220

Sparks RSJ, Burski MI, Carey SN, Gilbert JS, Glaze LS, Sigurdsson H, Woods AW (1997) Volcanic Plume. John Wiley & Sons, New York

Spillar V, Dolejs D (2013) Calculation of time-dependent nucleation and growth rates from quantitative textural data: inversion of crystal size distribution. J Petrol. doi:10.1093/petrology/egs091

Stovall WK, Houghton BF, Gonnermann HM, Fagents S.A, Swanson DA (2011) Eruption dynamics of Hawaiian-style fountains: The case study of episode 1 of the Kīlauea Iki 1959 eruption. Bull Volcanol 73:511–529. doi:10.1007/s00445-010-0426-z

Stovall WK, Houghton BF, Hammer JE, Fagents SA, Swanson DA (2012) Vesiculation of high fountaining Hawaiian eruptions: Episodes 15 and 16 of 1959 Kīlauea Iki. Bull Volcanol 74:441–455. doi:10.1007/s00445-011-0531-7

Streck MJ (2008) Mineral textures and zoning as evidence for open system processes. In Putirka KD, Tepley FJ (Eds) Minerals, inclusions and volcanic processes. Rev Mineral Geochem 69:595-622

Suzuki Y, Nakada S (2001) Timing of vesiculation and crystallization during magma ascent - Example of the phreatomagmatic phase in Usu 2000 eruption. Bull Earthq Res Inst 76:253-268

2539 Suzuki Y, Nakada S (2002) Vesiculation and magma ascent process in the Usu 2000 eruption,
2540 inferred from texture and size distribution of bubbles. Bull Volcanol Soc Japan 47:675-688
2541
2542 Swanson DA, Wooten K, Orr T (2009) Buckets of ash track tephra flux from Halemaʻumaʻu
2543 crater, Hawaii. Eos Trans AGU 90:427–428. doi:10.1029/2009EO460003
2544
2545 Szramek L, Gardner JE, Larsen J. (2006) Degassing and microlite crystallization of basaltic
2546 andesite magma erupting at Arenal Volcano, Costa Rica. J Volcanol Geotherm Res 157:182-
2547 201
2548
2549 Taddeucci J, Pompilio M, Scarlato P (2002) Monitoring the explosive activity of the July–
2550 August 2001 eruption of Mt. Etna (Italy) by ash characterization. Geophys Res Lett
2551 29(8):1029–1032. doi:10.1029/2001GL014372
2552
2553 Taddeucci J, Pompilio M, Scarlato P (2004) Conduit processes during the July–August 2001
2554 explosive activity of Mt. Etna (Italy): inferences from glass chemistry and crystal size
2555 distribution of ash particles. J Volcanol Geotherm Res 137:33–54
2556
2557 Taddeucci J, Scarlato P, Capponi A, Del Bello E, Cimarelli C, Palladino D, Kueppers U
2558 (2012) High-speed imaging of Strombolian explosions: The ejection velocity of pyroclasts.
2559 Geophys Res Lett 39(2)
2560
2561 Takeuchi S, Nakashima S (2005) A new simple gas permeameter for permeability
2562 measurement of small samples of volcanic eruptive material and experimental run products
2563 (in Japanese with English abstract). Bull Volcanol Soc Jpn 50:1–8
2564
2565 Takeuchi S, Nakashima S, Akihiko Tomiya A (2008) Permeability measurements of natural
2566 and experimental volcanic materials with a simple permeameter: toward an understanding of
2567 magmatic degassing processes. J Volcanol Geotherm Res 177:329–339.
2568 http://dx.doi.org/10.1016/j.jvolgeores.2008.05.010.
2569
2570 Tarquini S, Favalli M (2010) A microscopic information system (MIS) for petrographic
2571 analysis. Comput Geosci 36:665–674
2572

Thomas N, Jaupart C, Vergniolle S (1994) On the vesicularity of pumice. J Geophys Res 99:15633–15644

Thomas HE, Watson IM, Carn SA, Alfredo AJ, Prata F, Realmuto VJ (2011) A comparison of AIRS, MODIS and OMI sulphur dioxide retrievals in volcanic clouds. Geomatics, Nat Hazards Risk 2(3):217-232

Thordarson T, Self S, Larsen G, Rowland SK, Hoskuldsson A (2009) Studies in Volcanology: the Legacy of George Walker. GSL Special Publication

Toramaru A (1989) Vesiculation process and bubble size distribution in ascending magmas with constant velocities. J Geophys Res 94(1):523–17,542. doi:10.1029/JB094iB12p17523

Toramaru A (1990) Measurement of bubble size distributions in vesiculated rocks with implications for quantitative estimates of eruption processes. J Volcanol Geotherm Res 43:71–90

Toramaru A (2006) BND (bubble number density) decompression rate meter for explosive volcanic eruptions J Volcanol Geotherm Res 154:303-316

Toramaru A, Noguchi S, Oyoshihara S, Tsune A (2008) MND (microlite number density) water exsolution rate meter. J Volcanol Geotherm Res 175(1–2):156–167

Tsukui M, Suzuki Y (1995) Vesiculation of basaltic magma: magmatic versus phreatomagmatic eruption in 1983 eruption of Miyakejima. Bull Volcanol Soc Jpn 40, 395–399

Valade S, Donnadieu F (2011) Ballistics and ash plumes discriminated by Doppler radar. Geophys Res Lett 38:L22301. doi:10.1029/2011GL049415

Valade SA, Harris AJL, Cerminara M (2014) Plume Ascent Tracker: Interactive Matlab software for analysis of ascending plumes in image data. Comput Geosci 66:132–144. doi: 10.1016/j.cageo.2013.12.015

2607 Villemant B, Boudon G (1998) Transition between dome-forming and plinian eruptive styles:
2608 H20 and CL degassing behaviour. Nature 392:65-69
2609
2610 Vinkler AP, Cashman K, Giordano G, Groppelli G (2012) Evolution of the mafic Villa Senni
2611 caldera-forming eruption at Colli Albani volcano, Italy, indicated by textural analysis of
2612 juvenile fragments. J Volcanol Geotherm Res 235-236:37–54
2613
2614 Vlastélic I, Staudacher T, Bachèlery P, Télouk P, Neuville D, Benbakkar M (2011) lithium
2615 isotope fractionation during magma degassing: constraints from silicic differentiates and
2616 natural gas condensates from Piton de la Fournaise volcano (Réunion Island). Chem Geol
2617 284:26-34
2618
2619 Voltolini M, Zandomeneghi D, Mancini L, Polacci M (2011) Texture analysis of volcanic rock
2620 samples: Quantitative study of crystals and vesicles shape preferred orientation from X-ray
2621 microtomography data. J Volcanol Geot Res 202:83–95
2622
2623 Vöge M, Hort M, Seyfried R (2005) Monitoring volcano eruptions and lava domes with
2624 Doppler radar. EOS Trans AGU 86:537-541
2625
2626 Walker JC, Carboni E, Dudhia A, Grainger RG (2012) Improved detection of sulphur dioxide
2627 in volcanic plumes using satellite-based hyperspectral infrared measurements: Application to
2628 the Eyjafjallajökull 2010 eruption. J Geophys Res 117:D00U16. doi:10.1029/2011JD016810
2629
2630 Wallace PJ (2001) Volcanic SO_2 emissions and the abundance and distribution of exsolved gas
2631 in magma bodies. J Volcanol Geotherm Res 108:85-106
2632
2633 Wallace PJ (2005) Volatiles in subduction zone magmas: concentrations and fluxes based on
2634 melt inclusion and volcanic gas data. J Volcanol Geotherm Res 140:217-240
2635
2636 Watson IM, Realmuto VJ, Rose WI, Prata AJ, Bluth GJS, Gu Y, Bader CE, Yu T (2004)
2637 Thermal infrared remote sensing of volcanic emissions using the moderate resolution imaging
2638 spectroradiometer. J Volcanol Geotherm Res 135:75–89
2639

2640 Wen S, Rose WI (1994) Retrieval of sizes and total masses of particles in volcanic clouds
2641 using AVHRR bands 4 and 5. J Geophys Res: Atmospheres 99(D3):5421–5431
2642
2643 White JDL, Houghton BF (2006) Primary volcaniclastic rocks. Geology 34:677-680.
2644 doi:10.1130/G22346.1
2645
2646 Whitham AG, Sparks RSJ (1986) Pumice. Bull Volcanol 48:209–223
2647
2648 Wilhelm S, Worner, G (1996) Crystal size distribution in Jurassic Ferrar flows and sills
2649 (Victoria Land, Antarctica): Evidence for processes of cooling, nucleation, and crystallisation.
2650 Contrib Mineral Petr 125:1-15
2651
2652 Williams-Jones G, Stix J, Hickson C (2008) The COSPEC cookbook. IAVCEI: Methods in
2653 Volcanology I: 233 p.
2654
2655 Wilson L, Huang TC (1979) The influence of shape on the atmospheric settling velocity of
2656 volcanic ash particles. Earth Planet Sci Lett 44:311–324
2657
2658 Wilson L, Self S (1980) Volcanic explosion clouds: density, temperature and particle content
2659 estimates from cloud motion. J Geophys Res 85:2567-2572
2660
2661 Wright HMN, Weinberg R (2009) Strain localization in vesicular magma: Implications for
2662 rheology and fragmentation. Geology 37:1023–1026. doi:10.1130/G30199A.1
2663
2664 Wright HMN, Cashman KV (2014) Compaction and gas loss in welded pyroclastic deposits
2665 as revealed by porosity, permeability, and electrical conductivity measurements of the Shevlin
2666 Park Tuff. GSA Bulletin 126(1/2):234–247. doi: 10.1130/B30668.1
2667
2668 Wright HMN, Roberts JJ, Cashman KV (2006) Permeability of anisotropic tube pumice:
2669 model calculations and measurements. Geophys Res Lett 33:L17316.
2670 doi.org/10.1016/j.epsl.2009.01.023
2671

2672 Wright HMN, Cashman KV, Rosi M, Cioni R (2007) Breadcrust bombs as indicators of
2673 Vulcanian eruptiondynamics at Guagua Pichincha volcano. Ecuador. Bull Volcanol 69: 281–
2674 300
2675
2676 Wright HMN, Cashman KV, Gottesfeld EH, Roberts JJ (2009) Pore structure of volcanic
2677 clasts: Measurements of permeability and electrical conductivity. Earth Planet Sci Lett
2678 280:93–104. doi.org/10.1016/j.epsl.2009.01.023
2679
2680 Wright HMN, Folkes CB, Cas RAF, Cashman KV (2011) Heterogeneous pumice populations
2681 in the 2.08-Ma Cerro Galán Ignimbrite: implications for magma recharge and ascent
2682 preceding a large-volume silicic eruption. Bull Volcanol 73:1513–1533
2683
2684 Wright HMN, Cashman KV, Mothes PA, Hall ML, Ruiz AG, Le Pennec J-L (2012) Estimating
2685 rates of decompression from textures of erupted ash particles produced by 1999-2006
2686 eruptions of Tungurahua Volcano, Ecuador. Geology 40:619-622. doi:10.1130/G32948
2687
2688 Wohletz K (1983) Mechanisms of hydrovolcanic pyroclast formation: grainsize, scanning
2689 electron microscopy, and experimental studies. J Volcanol Geother Res 17:31–63
2690
2691 Wohletz K (1986) Explosive magma–water interactions: thermodynamics, explosion
2692 mechanisms, and field studies. Bull Volcanol 48:245–264
2693
2694 Wohletz K (1987) Chemical and textural surface features of pyroclasts from hydrovolcanic
2695 eruption sequences. In: Marsall, J.R. (Ed.), Clastic Particles. Van Nostrand Reinhold Co, New
2696 York, N.Y., pp. 79–97
2697
2698 Yang K, Krotkov NA, Krueger AJ, Carn SA, Bhartia PK, Levelt PF (2007) Retrieval of large
2699 volcanic SO2 columns from the Aura Ozone Monitoring Instrument (OMI): comparison and
2700 limitations. J Geophys Res 112:D24S43. doi:10.1029/2007JD008825
2701
2702 Yamada K, Emori H, Nakazawa K (2008) Time-evolution of bubble formation in a viscous
2703 liquid. Earth Planets Space 60:1–19
2704

Yokoyama T, Takeuchi S (2009) Porosimetry of vesicular volcanic products by a water-expulsion method and the relationship of pore characteristics to permeability. J Geophys Res 114:B02201. http://dx.doi.org/10.1029/2008JB005758.

Yoshimoto M, Shimano T, Nakada S, Koyama E, Tsuji H, Iida A, Kurokawa M, Okayama Y, Nonaka M, Kaneko T, Hoshizumi H, Ishizuka Y, Furukawa R, Nogami K, Onizawa S, Niihori K, Sugimoto T, Nagai M (2005) Mass estimation and characteristics of ejecta from the 2004 eruption of Asama volcano. Bull Volcanol, Soc Jpn 50:519–533 (In Japanese with English abstract)

Zandomeneghi D, Voltolini M, Mancini L, F. Brun, D. Dreossi, M. Polacci (2010) Quantitative analysis of X-ray microtomography images of geomaterials: Application to volcanic rocks, Geosphere, special issue "Advances in 3D Imaging and Analysis of Geomaterials" 6:793-804. doi:10.1130/GES00561.1.

Zakšek K, Hort M, Zaletelj J, Langmann B (2013) Monitoring volcanic ash cloud top height through simultaneous retrieval of optical data from polar orbiting and geostationary satellites. Atmos Chem Phys 13(5):2589-2606

Zimanowski B, Wohletz K, Dellino P, Buttner R (2003) The volcanic ash problem J. Volcanol. Geotherm. Res. 122:1-5

Zobin VM, Santiago-Jiménez H, Ramírez-Ruiz JJ, Reyes-Dávila GA, Bretón-González M, Navarro-Ochoa C (2007) Quantification of volcanic explosions from tilt records: Volcán de Colima, México. J Volcanol Geotherm Res 166(2):117-124

Figure captions

Figure 1 Diagrammatic illustration showing a volcanic strombolian conduit (modified from Harris and Ripepe 2007), and the list of a few parameters that can be measuremed trought the deposit (D), the texture of the pyroclasts (T), the geochemistry (G) and the geophysics (G) methods for small, magmatic explosions.

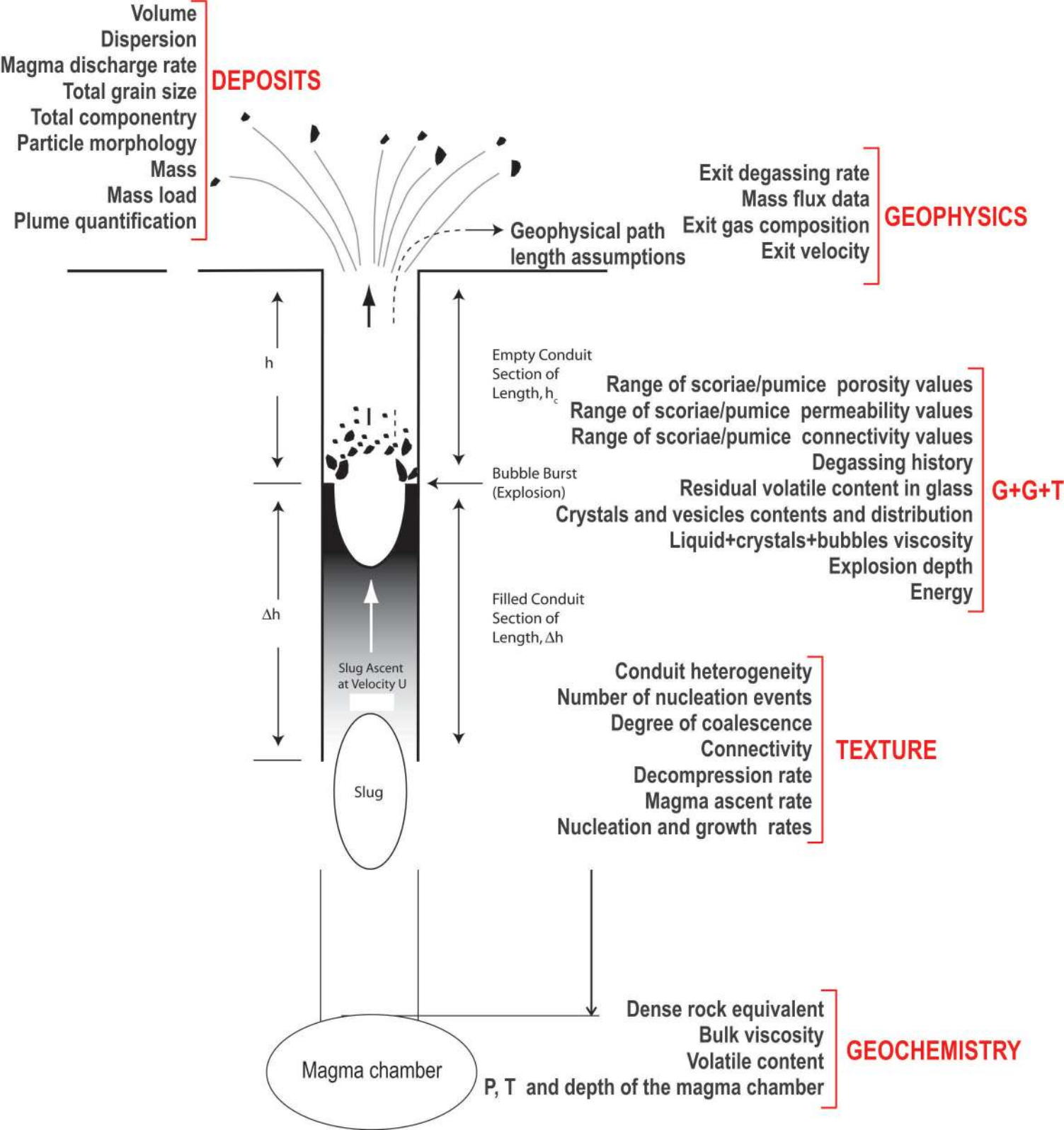

Volume
Dispersion
Magma discharge rate
Total grain size
Total componentry
Particle morphology
Mass
Mass load
Plume quantification
DEPOSITS
Geophysical path length assumptions
Exit degassing rate
Mass flux data
Exit gas composition
Exit velocity
GEOPHYSICS
h
Empty Conduit Section of Length, h_c
Range of scoriae/pumice porosity values
Range of scoriae/pumice permeability values
Range of scoriae/pumice connectivity values
Degassing history
Residual volatile content in glass
Crystals and vesicles contents and distribution
Liquid+crystals+bubbles viscosity
Explosion depth
Energy
G+G+T
Bubble Burst (Explosion)
Δh
Filled Conduit Section of Length, Δh
Slug Ascent at Velocity U
Slug
Conduit heterogeneity
Number of nucleation events
Degree of coalescence
Connectivity
Decompression rate
Magma ascent rate
Nucleation and growth rates
TEXTURE
Magma chamber
Dense rock equivalent
Bulk viscosity
Volatile content
P, T and depth of the magma chamber
GEOCHEMISTRY

Table 1 Quantification of explosive dynamics from textural parameters of the pyroclast components

Textural parameters	*Quantification*		*References*
Clast shape, morphology and size	Discriminate between different fragmentation mechanisms		Wohletz 1983; 1986; 1987; Heiken and Wohletz 1985; Sheridan and Marshall 1983; 1987; Dellino and La Volpe 1996a; b; Palladino and Taddeucci 1998; Büttner et al. 1999; 2002; Kueppers et al. 2006; Dellino et al. 2001; 2012; Zimanowski et al. 2003 Németh 2010 Pardo et al. 2014a
	Conduit stratigraphy and processes		Taddeucci et al. 2002; D'Oriano et al. 2005; Cioni et al. 2011; Perugini et al. 2011; Andronico et al. 2009b; 2013a; Lautze et al. 2012; 2013; Perugini et al. 2002;2007
	State of the magma at the fragmentation		Carey et al. 2000; Dellino and Liotino 2002; Maria and Carey 2002; 2007; D'Oriano et al. 2011; Ruth and Calder 2014
	Link between vesicularity and particle morphology, and particle morphology with cloud dispersal and sedimentation		Wilson and Huang 1979; Dellino et al. 2005; Mattsson 2010 Alfano et al. 2011; Mele et al. 2011
Clast density and vesicularity	Lateral variability of magma within the conduit		Houghton and Wilson 1989; Kennedy et al. 2005; Kueppers et al. 2005; Mueller et al. 2011; Barker et al. 2012
	Dense juvenile	Presence of outgassed magma	Sable et al. 2006; Lautze and Houghton 2005; 2007; 2008; Polacci et al. 2008; 2009a; b; 2012; Gurioli et al. 2005; 2014; Shea et al. 2011; 2012; 2014; Cimarelli et al. 2010
		Presence of a plug	Hoblitt and Harmon 1993; D'Oriano et al. 2005; Sable et al. 2009; Adams et al. 2006a; 2006b; Giachetti et al. 2010; Barker et al. 2012; Lavallée et al. 2012
Clast permeability and connectivity	Degassing history experienced by the magma		Eichelberger et al. 1986; Klug and Cashman 1996; Saar and Manga 1999; Jouniaux et al. 2000; Blower 2001a, b; Klug et al. 2002; Melnik and Sparks 2002; Rust and Cashman 2004; 2011; Mueller et al. 2005; 2008; Wright et al. 2006; 2007; 2009; Plats et al. 2007; Bernard et al. 2007; Takeuchi et al. 2008; Nakamura et al. 2008; Bouvet de Maisonneuve et al. 2009; Yokoyama and Takeuchi 2009; Bai et al. 2010; 2011; Degruyter et al. 2010a; 2010b; 2012

		Vinkler et al. 2012; Polacci et al. 2012; 2014; Nguyen et al. 2014; Pioli et al. 2008; Formenti and Druitt 2003; Giachetti et al. 2010; Shea et al. 2011; 2012
Clast conductivity	Input parameters for numerical percolation simulations	Le Pennec et al; 2001; Bernard et al. 2007; Wright et al. 2009; Wright et Cashman 2014
Vesicle shape and size	Bubble coalescence, ripening or collapse signatures	Klug and Cashman 1996; Mangan and Cashmann 1996; Gurioli et al. 2005; Shin et al. 2005; Sable et al. 2006; Polacci et al. 2008; Castro et al. 2012
	Shear conditions in the conduit Convection in the conduit	Marti et al. 1999; Polacci et al. 2001; 2003; Rust et al. 2003; Okumura et al. 2006; 2008; Bouvet de Maisonneuve et al. 2009; Wright and Weinberg 2009; Laumonier et al. 2011; Shea et al. 2011; 2012 Carey et al. 2013
	Eruptive style	Moitra et al. 2013
Vesicle size distributions (VSDs)	Vesicle nucleation processes and growth in magmas	Klug and Cashman 1994; Shea et al 2010a; LaRue et al. 2013, and references therein
	Total number of nucleation, coalescence or ripening events	Gaonac'h et al. 1996a; b Klug and Cashman 1996; Herd and Pinkerton 1997; Blower et al. 2001; 2002; Gaonac'h et al. 2003; 2005; Lovejoy et al. 2004, Yamada et al. 2008; Bai et al. 2008; Costantini et al. 2010
	Post-fragmentation evolution as indicator of : i) fountaining mechanisms ii) transportation and dispersal of the pyroclasts in submarine environment	Polacci et al; 2006a; Gurioli et al; 2008; Stovall et al. 2011; 2012; Schipper at al. 2010a, b, c; 2011; 2012; Rotella et al. 2013; 2014
Vesicle Number density (Nv)	Link with magma mass eruption rate (MER), link with column height	Polacci et al. 2006b; Toramaru 2006; Gurioli et al. 2008; Carey et al. 2009; Houghton et al. 2010; Rust and Cashman 2011; Alfano et al. 2012
	Magma decompression rate	Mangan and Sisson 2000; Suzuki and Nakada 2001; 2002; Toramaru 2006; Cluzel et al. 2008; Shea et al. 2010b; 2011; 2012; Wright et al. 2012
	Phreatomagmatic fragmentation	Tsukui and Suzuki 1995; Suzuki, Nakada 2001, 2002; Shimano and Nakada 2006; Mattsson 2010; Murtagh et al. 2011; Murtagh and White 2013
	Link vesicularity with external trigger mechanisms (crystallinity, pressure changes)	Belien et al. 2010; Carey et al. 2012; Gurioli et al. 2014

Crystal size distribution (CSD)	Crystal size (mean, modal, and maximum crystal size), crystallization kinetics (nucleation and growth rates), annealing, crystal accumulation, and fractionation	Cashman and Marsh, 1988; Marsh 1988; 1998; 2007; Cashman 1993; Armienti et al. 1994; Higgins 2000; 2002a;b; 2006; 2011; Wilhelm and Worner, 1996; Bindeman 2003; Gualda 2006; Gualda and Rivers 2006; Mock et al. 2003; Simakin and Bindeman, 2008; Spillar and Dolejs 2013
	Magma ascent rate	Cashman 1992; Rutherford and Hill 1993; Rutherford and Devine 2003; Noguchi et al. 2008; D'Oriano et al. 2011
	Pre-eruptive decompression paths	Hammer et al. 1999; Szramek et al. 2006; Clarke et al. 2007; Innocenti et al. 2013
	Magma storage conditions prior to eruption and residence times	Mangan 1990; O'Driscoll et al. 2007; Cigolini et al. 2008 Simakin and Bindeman 2008; Magee et al. 2010; Shea et al. 2009
	Water exsolution rate meter	Toramaru et al. 2008
	Magma mixing	Morgan et al. 2007; Jerram et al. 2003
Crystal+Vesicle size and percentage	Three phases magma rheology, fluid mechanical behavior of magma	Gurioli et al. 2014; Noguchi et al. 2006